

Supporting Information

for *Environmental Science & Technology*

Reactivity of bromine radical with dissolved organic matter moieties and monochloramine: Effect on bromate formation during ozonation

Sungeun Lim,^{1†} Benjamin Barrios,² Daisuke Minakata,² Urs von Gunten^{1,3*}

¹Eawag, Swiss Federal Institute of Aquatic Science and Technology, Ueberlandstrasse 133, 8600 Duebendorf, Switzerland

²Department of Civil and Environmental Engineering, Michigan Technological University, 1400 Townsend Drive, Houghton, Michigan 49931, United States

³School of Architecture, Civil and Environmental Engineering (ENAC), École Polytechnique Fédérale de Lausanne (EPFL), 1015 Lausanne, Switzerland

[†]Current address: Department of Civil and Environmental Engineering, Stanford University, 473 Via Ortega, Stanford, CA 94305, United States

*Corresponding author: vongunten@eawag.ch, phone: +41 58 765 5270

This **Supporting Information** includes 18 texts, 10 tables, 21 figures, and 1 scheme in 45 pages.

Table of contents

Text S1. Chemical reagents and stock solutions	S6
Text S2. Preparation of DOM stock solution.....	S6
Text S3. Preparation of chloride-free monochloramine (NH ₂ Cl) stock solutions	S6
Text S4. Dosimetry	S7
Text S5. Sample preparation for kinetic experiments performed with γ -radiolysis	S8
Text S6. Dissolved O ₂ in γ -radiolysis samples.....	S9
Text S7. Masking bromide by Ag ⁺	S9
Text S8. Adapted competition kinetics for determining $k_{Br^{\bullet}}$ of DOM and NH ₂ Cl.....	S10
Text S9. Sample preparation for γ -radiolysis for phenol-Br [•] reaction experiments.....	S10
Text S10. Chromatographic methods	S11
Text S11. Ozonation experiment	S12
Text S12. Quantum chemical calculation methods	S12
Text S13. Validation of quantum chemical calculation methods	S13
Text S14. Calculation of free energy of activation by the Marcus theory	S13
Text S15. LC-HRMS/MS evidences supporting the formation of C ₆ H ₃ BrO ₃ and C ₆ H ₅ BrO ₃ for the phenol-Br [•] reaction	S14
Text S16. Formation pathway of 4-bromophenol from the phenol-Br [•] reaction.....	S15
Text S17. Principles of the chlorine-ammonia pretreatment as a bromate mitigation strategy of ozonation	S16
Text S18. Calculation of the fractions of Br [•] -related reactions during ozonation	S16
Table S1. Chemical reagents	S18
Table S2. Compounds analyzed by HPLC and LC-HRMS/MS and the corresponding analytical condition and LOQ.	S19
Table S3. Detected exact masses and mass deviation by LC-HRMS/MS.	S19
Table S4. Theoretically calculated $\Delta G_{\text{solv,calc}}$ values and experimental values of halides and halogen radicals in kcal/mol. n is the number of explicit water molecule(s).	S20

Table S5. Benchmark calculations of one electron reduction potential of Br [•] /Br ⁻	S20
Table S6. Validation of one electron reduction potential for selected organic compounds at the M06-2X/Aug-cc-pVDZ//M06-2X/Aug-cc-pVTZ level of theory with the SMD solvation model	S20
Table S7. Calculated free energy of adduct formation ($\Delta G^{\text{adduct}}_{\text{aq}}$) for the reactions of organic model compounds with Br [•] (red sphere) and the optimized molecular structures of the adducts.....	S21
Table S8. Compiled QC calculation results for the reactions of the selected organic model compounds and of NH ₂ Cl with Br [•] ($\Delta G^{\text{react}}_{\text{aq,calc}}$ as the standard state aqueous phase free energy of reaction, λ as the reorganization energy, and $\Delta G^{\text{act}}_{\text{aq,SET}}$ as the aqueous phase free energy of activation).	S25
Table S9. Spin density distribution of protonated and deprotonated forms of benzylamine and <i>N,N</i> -dimethylbenzylamine.....	S27
Table S10. Scavenging rates ($k_{\text{species}}, \text{s}^{-1}$) of e ⁻ , [•] OH, [•] H, Br [•] , and [•] tBA (<i>t</i> -butanol derived radical) by the reaction species in γ -radiolysis kinetic experiments (1,2-dibromoethane (1,2-DBE), Ag ⁺ , <i>t</i> -butanol, a model compound, phosphate ions (H ₂ PO ₄ ⁻ /HPO ₄ ²⁻ for pH 7), and dissolved O ₂), based on the reported or assumed second-order rate constants ($k_{\text{species}}, \text{M}^{-1}\text{s}^{-1}$) and the applied concentrations (conc., M) ..	S27
Figure S1. Total chloride concentrations ([Cl ⁻] _{tot}) of primary NH ₂ Cl stock solutions after reducing NH ₂ Cl by sulfite. [Cl ⁻] _{tot} indicates the sum of the chloride concentration already present in the stock solution and chloride formed from the reduction of NH ₂ Cl with sulfite. The NH ₂ Cl concentration of the stock solution was 0.38 mM.....	S28
Figure S2. Left: Determined and theoretical NH ₂ Cl concentrations in supernatant of the silver(I)-treated NH ₂ Cl stock solutions (as 0.4mM, 1.7mM and 3.5mM NH ₂ Cl); right: measured chloride concentrations in 0.2 mM NH ₂ Cl solutions prepared by diluting 0.4, 1.7, or 3.5 mM NH ₂ Cl stock solutions and reducing NH ₂ Cl of each solution by sulfite.....	S28
Figure S3. Setup for preparing γ -radiolysis samples for the competition kinetics experiments. To transfer the Ar-saturated solution to the sample vials containing an air-saturated solution (shown as 1.5mL amber vials with crimp neck), the transferring tubing was placed to the bottom of the vials.	S29
Figure S4. Flow charts of the sample preparation for kinetic experiments performed with γ -radiolysis for (a) most organic model compounds, (b) <i>p</i> -benzoquinone, and (c) benzene, toluene, and naphthalene. DBE stands for 1,2-dibromoethane. Background shades separate the days on which an individual step (preparation, γ -radiolysis, and analyses) was carried out.	S30

Figure S5. Competition kinetics plots for the reactions of Br[•] with the organic model compounds, NH₂Cl, DOM, and oxidized DOM (by 0.8 gO₃/gC or 1.5 gO₃/gC) at pHs 7.1 or 10.2. Concentrations of the model compounds were fixed at 3.0 – 3.4 μM. Concentrations of NH₂Cl, DOM, and oxidized DOM are stated in the figure headings. Data points are from a single measurement and *k*_{Br[•]} was calculated mostly based on an average of experimental duplicates..... S33

Figure S6. Slopes obtained by linear regression of data points of the competition kinetics plots (shown in Figure S5) as a function of a reciprocal of the DOC or NH₂Cl concentration, to derive *k*_{Br[•]} for NH₂Cl, DOM, and oxidized DOM (by 0.8 gO₃/gC or 1.5 gO₃/gC). See Text S8 for the corresponding rate expression.S34

Figure S7. Quantitative structure-activity relationship of the measured *k*_{Br[•]} of the selected aromatic model compounds with (a) Hammett constants and (b) computed activation energies..... S34

Figure S8. Schematic reaction coordinate for the reaction of phenol with Br[•]..... S35

Figure S9. Correlation between the measured *k*_{Br[•]} of the selected organic model compounds and aqueous phase free energies for the formation of adducts ($\Delta G^{\text{adduct}}_{\text{aq}}$). S35

Figure S10. Concentrations of phenol and the identified products as a function of the γ -radiolysis time during the reaction of phenol with Br[•], for the condition with 22 μM phenol, 0.7 mM 1,2-dibromoethane, 40 mM *t*-butanol, and 50 mM phosphate buffer (pH 7.1). See Figure 2 (main text) for relative product formation. S36

Figure S11. Left: Filtered chromatograms of a blank sample (no γ -radiolysis); right: γ -radiolysis sample (t = 40 min) with exact masses of 200.9193, 202.9172, 202.9349, and 204.9329 (from top to bottom of the chromatograms) corresponding to the molecular formulas of C₆H₃⁷⁹BrO₃, C₆H₃⁸¹BrO₃, C₆H₅⁷⁹BrO₃, and C₆H₅⁸¹BrO₃. S36

Figure S12. Trends of the peak intensity as a function of the γ -radiolysis time for the exact masses of 200.9193 (blue circles, corresponding to C₆H₂⁷⁹BrO₃ as M-H) and 202.9349 (orange triangles, corresponding to C₆H₄⁷⁹BrO₃ as M-H) during the reaction of Br[•] with phenol (left) or *p*-benzoquinone (right). S37

Figure S13. Left: Filtered chromatograms of a γ -radiolysis sample (t = 40 min); right: synthesized substituted *p*-benzoquinone with the exact masses of 200.9193, 202.9172, 202.9349, and 204.9329 (from top to bottom of the chromatograms) as [M-H], corresponding to the molecular formulas C₆H₃⁷⁹BrO₃, C₆H₃⁸¹BrO₃, C₆H₅⁷⁹BrO₃, and C₆H₅⁸¹BrO₃. Retention times for C₆H₃BrO₃, and C₆H₅BrO₃ are 7.8

and 6.1 min for the γ -radiolysis sample (left) and 11.9 and 8.7 min for the synthesized chemical (right).
..... S37

Figure S14. MS² spectra of m/z of 123.0089 (as [M-H]) with a HCD normalized collision energy (unitless) of 15 (top), 45 (middle), or 60 (bottom). S38

Figure S15. Simulated fragment ions corresponding to the detected major daughter ions of m/z = 95.0140 and 68.9974. Two different suspected structures are shown for the parent ion of 123.0089 as [M-H]. The fragment ions were obtained based on an *in silico* fragmentation simulation by MetFrag.⁴⁸
..... S38

Figure S16. Top: Measured; bottom: reported MS² spectra for the exact masses of 185.0610 and 185.0608, respectively (both corresponding to C₁₂H₉O₂ as M-H). The reported MS² spectrum was obtained from <https://massbank.eu/MassBank/>.⁴⁹ S39

Figure S17. Resonance structures of the phenoxy radical..... S39

Figure S18. Calculated fractions of Br[•] reacting with DOM (green line), ozone (red line), bromide (blue line), or NH₂Cl (orange line) as a function of the ozone concentration in (a) absence or (b) presence of NH₂Cl. The selected concentrations were 5 mgC/L DOC, 1.3 μ M Br⁻ (100 μ g/L Br⁻), and 15 μ M NH₂Cl.S40

Figure S19. Calculated fractions of Br[•] reacting with NH₂Cl as a function of (a) bromide, (b) ozone, or (c) DOC concentration. Lines indicate modelled NH₂Cl concentrations (1, 2, 5, 10, and 15 μ M) and an asterisk symbol indicates the conditions applied in the ozonation experiment. Bromide, ozone, and DOC concentrations were fixed at 2 μ M, 60 μ M, and 1.4 mgC/L (corresponding to the experimental conditions) when they were not an independent variable of the plot. S40

Figure S20. (a) *p*CBA abatement as a function of the ozone exposure and (b) ozone decrease as a function of reaction time, for ozonation of Lake Zurich water (1.4 mgC/L DOM, 2 μ M bromide, 1 mM phosphate buffer (pH 7.6), 5 μ M *p*CBA, and an ozone dose of 60 μ M in absence or presence of an additional agent (10 μ M formate, 4 μ M ammonium, 7 μ M NH₂Cl, or 15 μ M NH₂Cl). The numbers in parentheses in the legend in plot (a) indicate the R_{ct} derived from the slopes of the regression lines.S41

Figure S21. Fraction of Br[•] in equilibrium with BrOH^{-•} as a function of pH..... S41

Scheme S1. Possible initial reaction pathways for the reaction of phenol with Br[•]..... S42

References S43

Text S1. Chemical reagents and stock solutions

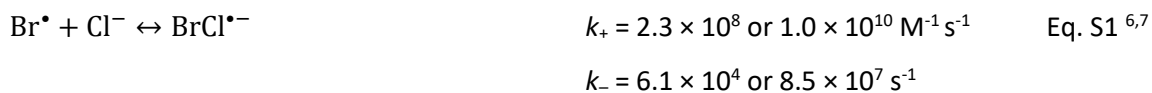
The chemical reagents used in this study are summarized in Table S1. Hypochlorite solution was standardized spectrophotometrically ($\epsilon_{290\text{nm}} = 350 \text{ M}^{-1} \text{ cm}^{-1}$).¹ Dissolved organic matter (DOM) and monochloramine (NH_2Cl) stock solutions were prepared as described in Text S2 and Text S3, respectively. All solutions were prepared in ultrapure water with a resistivity of 18.2 $\text{M}\Omega\cdot\text{cm}$. Lake Water Zurich was collected at Zurich Water Supply (Lengg) and filtered on the same day of collection with a cellulose nitrate filter (0.45 μm , Sartorius Stedim Biotech). General water quality parameters of the filtered Lake water were analyzed by the AuA laboratory (Eawag, Dübendorf) and summarized as follows: pH 8.3, alkalinity 2.69 mM, hardness 1.49 mM, bromide < 0.05 mg/L, nitrate 0.7 mg/L as NO_3^- -N, ammonium < 5.0 $\mu\text{g/L}$ as NH_4^+ -N, nitrite < 1.0 $\mu\text{g/L}$ as NO_2^- -N, and DOC 1.4 mg/L.

Text S2. Preparation of DOM stock solution

A 50 mgC/L DOM stock solution was prepared by dissolving the corresponding amount of Suwannee River Fulvic Acid II (2S101F, IHSS, 52.34%(w/w), <https://humic-substances.org/>) in 20 mM phosphate buffer at pH 7. The stock solution was standardized based on UV absorbance at 254nm after diluting 5 times.² An ozonated DOM stock solution was prepared with two ozone doses (0.8 gO_3/gC and 1.5 gO_3/gC) and ozone was completely consumed over night. Due to the dilution, the final concentrations of the oxidized DOM stock solutions were 33 mgC/L (0.8 gO_3/gC) and 26 mgC/L (1.5 gO_3/gC). To control the extent of oxidation, the electron donating capacity (EDC) of the DOM stock solutions was measured before and after ozonation by an EDC assay using the radical cation of 2,2'-azino-bis(3-ethylbenzothiazoline-6-sulfonate) (ABTS^{•+}) as described by Walpen et al. (2020).³ The decrease in EDC of the DOM stock solution after ozonation was (31 \pm 5)% for 0.8 gO_3/gC and (40 \pm 4)% for 1.5 gO_3/gC , in a similar range of previously reported EDC of ozonated DOM solutions.^{4,5}

Text S3. Preparation of chloride-free monochloramine (NH_2Cl) stock solutions

Hypochlorite solution contains high concentrations of chloride from the manufacturing process. The presence of chloride in NH_2Cl stock solution would interfere determining $k_{\text{Br}\cdot}$ of NH_2Cl , because chloride can react fast with $\text{Br}\cdot$ as shown in Eq. S1.



To prevent this interference, chloride in prepared NH_2Cl stock solution was removed by a following description. A primary NH_2Cl stock solution was prepared by mixing 15 mM of sodium hypochlorite (at

pH 9.5 by NaOH) with 7.5 mM of diammonium sulfate at a mixing ratio of 1:1 by a syringe pump with a speed of 1 mL/min. The resulting solution produced (6.9 ± 0.1) mM NH_2Cl as a main species with a negligible impurity of NHCl_2 (up to 0.1 mM), determined by UV absorbance at 245 and 295 nm and the corresponding molar absorptivity coefficients ($\epsilon_{245, \text{NH}_2\text{Cl}} = 445 \text{ M}^{-1} \text{ cm}^{-1}$, $\epsilon_{245, \text{NHCl}_2} = 208 \text{ M}^{-1} \text{ cm}^{-1}$, $\epsilon_{295, \text{NH}_2\text{Cl}} = 14 \text{ M}^{-1} \text{ cm}^{-1}$, $\epsilon_{295, \text{NHCl}_2} = 267 \text{ M}^{-1} \text{ cm}^{-1}$).⁸

To prepare a chloride-free NH_2Cl stock solution, the amount of chloride (Cl^-) present in the primary NH_2Cl stock solution was first determined by diluting the stock solution to 0.4 – 0.5 mM NH_2Cl , subsequently reducing NH_2Cl to Cl^- with sulfite, and measuring a total Cl^- concentration (as a sum of Cl^- present in the diluted stock and Cl^- reduced from NH_2Cl) by ion chromatography (Text S10). NH_2Cl was completely reduced by 1.0 – 1.5 molar equivalent of sulfite relative to NH_2Cl (Figure S1). The total $[\text{Cl}^-]$ was 1.4 – 1.6 mM in the diluted NH_2Cl stock solutions and therefore the $[\text{Cl}^-]$ already present in the solutions was 1.0 – 1.2 mM. After determining $[\text{Cl}^-]$, the primary NH_2Cl stock solution was again diluted to 0.4, 1.7, and 3.5 mM NH_2Cl and a 1.1 molar equivalent of silver (Ag^+) with regard to the inherent $[\text{Cl}^-]$ was added to the diluted NH_2Cl stock solutions to remove Cl^- . The silver-spiked solutions were allowed to sediment the precipitate (AgCl) for > 6 h. Afterwards, the supernatant was taken to measure $[\text{NH}_2\text{Cl}]$ by a DPD method⁹ to check an effect of the silver addition on $[\text{NH}_2\text{Cl}]$. The determined $[\text{NH}_2\text{Cl}]$ by DPD were within $\pm 3\%$ from the theoretical $[\text{NH}_2\text{Cl}]$ (except for the stock solution with the lowest $[\text{NH}_2\text{Cl}]$, 0.4 mM, deviated by 27%) (Figure S2a), and thus the effect was negligible. The supernatant was also taken to measure total $[\text{Cl}^-]$ by IC, by diluting the 0.4, 1.7, and 3.5 mM NH_2Cl stock solutions to 0.2 mM NH_2Cl and reducing NH_2Cl by sulfite. The measured $[\text{Cl}^-]$ were 0.18 – 0.19 mM, close to the theoretical $[\text{NH}_2\text{Cl}]$ (0.2 mM) (Figure S2b), indicating that only limited Cl^- is present in the supernatant of the NH_2Cl stock solutions. As a result, the supernatant of the silver-spiked NH_2Cl stock solution was used for determining k_{Br^\bullet} .

Text S4. Dosimetry

The dose rate was determined by an air-saturated 1 mM formate solution prepared in 2 mM phosphate buffer at pH 6.5 where all reactive species (solvated electron (e^-), $^{\bullet}\text{OH}$, H^{\bullet}) are converted to hydrogen peroxide.¹⁰ Hydrogen peroxide formed in the solution over time (0 – 15 min) was quantified spectrophotometrically by the Allen's reagent¹¹ and used to calculate the dose rate. The calculated dose rate was 0.13 kGy/h, corresponding to the electron formation rate ($fr(e^-)$) of 9.7 nM/s and the Br^\bullet formation rate ($fr(\text{Br}^\bullet)$) of 9.7 nM/s by assuming a 100% conversion of e^- to Br^\bullet (from the reaction of e^- with 1,2-dibromoethane).

Text S5. Sample preparation for kinetic experiments performed with γ -radiolysis

γ -radiolysis of aqueous solution produces e^- , $^{\bullet}\text{OH}$, H^{\bullet} , and H_2O_2 as reactive species with e^- and $^{\bullet}\text{OH}$ being the major species. For generating Br^{\bullet} , 1,2-dibromoethane was used, which forms Br^{\bullet} by the reaction with e^- , according to the Eqs. S2 and S3. The other major reactive species, $^{\bullet}\text{OH}$, was quenched by *t*-butanol to avoid interferences for the oxidation of probe compounds and guarantee a high yield of Br^{\bullet} from the reaction of 1,2-dibromoethane with e^- . The scavenging of e^- by 1,2-dibromoethane was at least 84% (depending on the dissolved O_2 concentration) of the total scavenging rate of e^- (Table S10).



The formed Br^{\bullet} is in equilibrium with hydroxide ($\text{BrOH}^{\bullet-} \leftrightarrow \text{Br}^{\bullet} + \text{HO}^-$, $K_{\text{eq}} = 3.2 \times 10^{-4} \text{ M}$)¹⁶ and therefore affected by pH. Under the pH conditions we applied (pH 7 and 10), the equilibrium clearly favors Br^{\bullet} , with the fraction of Br^{\bullet} as 100% and 76%, respectively. The fraction of Br^{\bullet} as a function of pH calculated based on the reported K_{eq} is shown in Figure S21.

Sample preparation is illustrated in Figure S3 for a setup image and in Figure S4 as flow charts. Samples for most organic model compounds (except *p*-benzoquinone, benzene, toluene, and naphthalene) were prepared one day prior to γ -radiolysis. 100 mL of solution containing 4 μM of ibuprofen, 4 μM of an organic model/target compound, and 50 mM phosphate buffer (pH 7.1) or 50 mM borate buffer (pH 10.2) was saturated with Ar gas. The Ar-saturated solution was then delivered to six 1.5 mL amber vials containing 0.21 mL of air-saturated solution of 5 mM of 1,2-dibromoethane and 29 mM of *t*-butanol, via a transferring tubing under N_2 gas flow, roughly until the neck of each vial (see Figure S3 for setup image). By mixing of Ar- and air-saturated solutions a certain level of dissolved oxygen (see below) could be achieved for the reasons described in Text S6. After the transfer, the vials were immediately closed with crimp caps to minimize gas exchange with the atmosphere. Mixed concentrations of the reactants in the vials were 3.4 μM ibuprofen, 3.4 μM target compound, 0.7 mM 1,2-dibromoethane, and 4 mM *t*-butanol. Each vial represented a designated γ -radiolysis time (0, 4, 8, 12, 16, and 20 min).

Samples for experiments with *p*-benzoquinone were prepared according to the description above, except that *p*-benzoquinone was added to the sample solution on site just before γ -radiolysis to minimize its loss. 10 μL of a 0.6 mM *p*-benzoquinone solution was added to roughly 1.5 mL of the pre-mixed solution containing ibuprofen, 1,2-dibromoethane, and *t*-butanol, using a glass syringe through the septum of the crimp caps. The weight of the vials was determined before and after adding *p*-

benzoquinone, to account for deviations in the final concentration of *p*-benzoquinone, caused by differences in sample volumes across the vials.

Samples for benzene, toluene, and naphthalene were prepared on site. 90 mL of a solution containing 3.3 μM ibuprofen and 50 mM phosphate buffer (pH 7.1) was placed in a 150 mL reaction vessel and saturated with Ar. 10 mL of an air-saturated solution containing 5 mM 1,2-dibromoethane and 20 mM *t*-butanol and 300 μL of 1 mM organic compound (benzene, toluene, or naphthalene) were added to the Ar-saturated solution and immediately placed in the γ -radiolysis source. The final concentrations of the reactants were 3 μM ibuprofen, 3 μM target compound, 0.5 mM 1,2-dibromoethane, and 2 mM *t*-butanol. During γ -radiolysis, 1 mL samples were taken every 4 min up to 20 min for further analyses.

Text S6. Dissolved O_2 in γ -radiolysis samples

O_2 concentrations were kept at a level to guarantee quenching of carbon-centered radicals derived from the reaction of *t*-butanol with $\cdot\text{OH}$ ($\cdot\text{tBA}$) during the radiolysis, which may oxidize target aromatic compounds,¹⁷ but still low enough not to quench too much e^- . The desired O_2 level was achieved by mixing Ar- and air-saturated solutions with a volumetric ratio of 6:1. O_2 concentrations were measured by an optical O_2 sensor (PreSens, Oxygen Microsensor NTH-PSt7). The average of O_2 concentrations measured immediately after the mixing were $(2.7 \pm 0.3) \% \text{O}_2$ saturation (equivalent to $(35 \pm 4) \mu\text{M O}_2$), which slightly increased to $(4.0 \pm 1.1) \% \text{O}_2$ saturation (or $(52 \pm 14) \mu\text{M O}_2$) after 15 hours storage at room temperature. For the O_2 concentration of $\sim 70 \mu\text{M}$ (highest possible O_2), the scavenging of e^- by O_2 was 11% of the total scavenging rate of e^- , while the scavenging of $\cdot\text{tBA}$ by O_2 was 92% of the total scavenging rate of $\cdot\text{tBA}$ (Table S10). The mixed solution was treated by γ -radiolysis within 24 hours to minimize reintroduction of O_2 .

Text S7. Masking bromide by Ag^+

The bromine radical ($\text{Br}\cdot$) was generated from the reaction of 1,2-dibromoethane with e^- (Eqs. S2 and S3). The reaction inherently forms Br^- as a side product (Eq. S2) which could quench $\text{Br}\cdot$ very efficiently (Eq. S4). To prevent this undesired $\text{Br}\cdot$ quenching, Br^- was masked by the fast reaction with silver(I) (Ag^+ , Eq. S5) by injecting 24 μL of 0.135 mM silver nitrate solution with a Hamilton glass syringe through a rubber septum of the 1.5 mL amber vials, after every 4 min of γ -radiolysis treatment (total 11 $\mu\text{M Ag}^+$ added for 20 min of γ -radiolysis, equivalent to the expected concentration of Br^- formed). Ag^+ was added in a distributed way to reduce a possibility of quenching $\text{Br}\cdot$ by Ag^+ (note that $k_{\text{Br}\cdot}$ of Ag^+ is not

available, but assumed high according to the $k_{\bullet\text{OH}}$ of Ag^+ as high as $10^{10} \text{ M}^{-1} \text{ s}^{-1}$).¹⁸ After the designated time (0 – 20 min with 4 min intervals), samples were taken out from the γ -radiation source and 40 μL of 26.5 mM sodium chloride was added to the vial to quench potentially residual Ag^+ . The same bromide-masking protocol was applied for the product analysis samples prepared in 11 mL vials, but with higher concentrations of the silver nitrate and sodium chloride stock solutions, to account for the larger volumes of the vials (i.e., 1 mM silver nitrate and 192 mM sodium chloride).



$$k_{-} = 3.1 \times 10^4 \text{ s}^{-1}$$



Text S8. Adapted competition kinetics for determining $k_{\text{Br}^{\bullet}}$ of DOM and NH_2Cl

$k_{\text{Br}^{\bullet}}$ of DOM was determined by measuring a decrease in ibuprofen over time under varying conditions with ibuprofen (1 μM) and DOC concentration variation in the range of 2 – 15 mgC/L. To derive $k_{\text{Br}^{\bullet}}$ of DOM, a steady-state concentration of Br^{\bullet} ($[\text{Br}^{\bullet}]_{\text{ss}}$) was assumed, where the formation rate ($fr(\text{Br}^{\bullet})$), governed by the dose rate of the γ -radiation source (Text S4)), is equal to the consumption rate as expressed in Eq. S6, with X as DOM. Eq. S6 can be rearranged for $[\text{Br}^{\bullet}]_{\text{ss}}$, which is then approximated to Eq. S7 for the condition where $k_{\text{Br}^{\bullet},\text{Ibu}}[\text{Ibu}] \ll k_{\text{Br}^{\bullet},\text{X}}[\text{X}]$ (X = DOM). Finally, $k_{\text{Br}^{\bullet}}$ of DOM is derived by plotting a slope obtained by a linear regression of the $\ln([\text{Ibu}]/[\text{Ibu}]_0)$ over time data (as shown in Figure S5) as a function of $1/[\text{DOM}]$ (as shown in Figure S6), based on Eq. S8. $k_{\text{Br}^{\bullet}}$ of NH_2Cl was determined accordingly but with varying $[\text{NH}_2\text{Cl}]$ in the range of 0.01 – 0.4 mM and with X as NH_2Cl in Eqs S6 – S8.

$$fr(\text{Br}^{\bullet}) = k_{\text{Br}^{\bullet},\text{Ibu}}[\text{Br}^{\bullet}]_{\text{ss}}[\text{Ibu}] + k_{\text{Br}^{\bullet},\text{X}}[\text{Br}^{\bullet}]_{\text{ss}}[\text{X}] \quad \text{Eq. S6}$$

$$[\text{Br}^{\bullet}]_{\text{ss}} = \frac{fr(\text{Br}^{\bullet})}{k_{\text{Br}^{\bullet},\text{Ibu}}[\text{Ibu}] + k_{\text{Br}^{\bullet},\text{X}}[\text{X}]} \approx \frac{fr(\text{Br}^{\bullet})}{k_{\text{Br}^{\bullet},\text{X}}[\text{X}]} \quad \text{Eq. S7}$$

$$\ln\left(\frac{[\text{Ibu}]}{[\text{Ibu}]_0}\right) = -k_{\text{Br}^{\bullet},\text{Ibu}}[\text{Br}^{\bullet}]_{\text{ss}}t = -\frac{k_{\text{Br}^{\bullet},\text{Ibu}}}{k_{\text{Br}^{\bullet},\text{X}}} \frac{fr(\text{Br}^{\bullet})t}{[\text{X}]} \quad \text{Eq. S8}$$

Text S9. Sample preparation for γ -radiolysis for phenol- Br^{\bullet} reaction experiments

Samples for product analyses for the reaction of phenol with Br^{\bullet} were prepared one day prior to γ -radiolysis similarly to the kinetic experiments but in larger volumes. 100 mL solution containing 25 μM of phenol and 50 mM phosphate buffer (pH 7.1) was saturated with Ar and brought to four 11 mL clear vials with 1.54 mL of air-saturated solution containing 5 mM of 1,2-dibromoethane and 286 mM of t-

butanol, via the setup described above. The final concentrations of the reactants in the vials were 22 μM phenol, 0.7 mM 1,2-dibromoethane, and 40 mM *t*-butanol. Ag^+ for masking bromide was added as described in Text S7. Samples were taken after 12, 20, and 40 min and analyzed by HPLC-DAD (or HPLC-FLD) and LC-HRMS/MS within 24 hours.

Text S10. Chromatographic methods

All kinetic and product samples from γ -radiolysis were filtered by a syringe filter (Nylon, 0.45 μm , 4 mm) prior to analyses. Most organic model compounds and phenol- Br^\bullet products (except those mentioned below) were analyzed by HPLC (Ultimate 3000, Thermo) equipped with diode array detector (DAD) and fluorescence detector (FLD) with a COSMOSIL 5C18-MS-II (3.0 \times 150 mm, 5 μm) column using a gradient method with methanol and 10 mM H_3PO_4 as eluents. The gradient started at 45% methanol (i.e., 55% H_3PO_4), gradually increased to 95% methanol for 20 min, stayed at 95% methanol for 4 min, returned to 45% methanol in 5 min, and remained at 45% methanol for 5.5 min (total analyzing time = 30 min). For hydroquinone and catechol, the same C18 column was used but with a different gradient: the gradient started at 5% methanol, increased to 95% for 25 min, stayed at 95% for 8.5 min, returned to 5% in 1 min, and remained at 5% for 5.5 min (total analyzing time = 40 min). For 3-phenylpropionic acid, the same C18 column was used but with different eluents (acetonitrile and 10 mM H_3PO_4) and a different gradient: the gradient started at 30% acetonitrile, increased to 60% for 13 min, stayed at 60% for 15 min, returned to 30% in 0.5 min, and remained at 30% for 6.5 min (total analyzing time = 36 min). For benzylamine and *N,N*-dimethylbenzylamine, a hydrophilic interaction liquid chromatography column (XBridge™ BEH HILIC XP, 2.5 μm particle size, 3.0 \times 150 mm, Waters) was used with an acetonitrile mixture (95:3:2 acetonitrile:methanol:water) and water as eluents. The gradient started at a 100% acetonitrile mixture for the first 2 min, decreased to 5% for 10 min, stayed at 5% for 5 min, returned to 100% in 1 min, and remained at 100% for 19 min (total analyzing time = 37 min). The flow rate was set at 0.4 mL/min for all analyses and the injection volume was 25 μL . The detector setup is summarized in Table S2.

Identified and suspected products for the reaction of phenol with Br^\bullet were analyzed by LC coupled with high resolution tandem mass spectrometer (Q Exactive, Thermo Scientific). LC separation was carried out with the same C18 column as above with a gradient method using ultrapure water and methanol (both with 0.1% formic acid) as eluents A and B, respectively. The gradient started with 5% B, gradually increased to 95% B for 25 min, held at 95% B for 8.5 min, returned to 5% B for 1 min, and was maintained at 5% B for 5.5 min. The total analyzing time was 40 min. The flow rate was 0.4 mL/min and

the injection volume was 25 μL . The MS detector was with electrospray ionization with either a full MS¹ scan mode (R = 35,000, mass range = 60 – 600 for all modes) with data-dependent MS² (R = 35,000) or a targeted MS² mode with an inclusion list specifying the masses of interest (corresponding to suspected phenol oxidation products) and a range of applied collision energies (15, 45, and 60 as (N)CE). Both modes were operated in positive or mostly negative polarity with a spray voltage of 4000 V (positive) or 3000 V (negative), a capillary temperature of 350 °C, a sheath gas flow rate of 40, and an auxiliary gas flow rate of 10. Detected exact masses of the phenol-Br[•] products and mass deviations are summarized in Table S3.

Samples containing chloride and bromate were first diluted with ultrapure water (100 times for chloride, 10 times for bromate) and analyzed by ion chromatography coupled with conductivity detector (Dionex™ Integrion™ HPIC™ System) with an anion exchange IC column (Dionex™ IonPac™ AS19-4 μm IC Column 2 \times 250mm with AG19-4 μm Guard Column 2 \times 50mm) with a gradient of KOH as eluent, starting at 10 mM for 10 min, gradually increasing to 30 mM for 20 min, increasing to 100 mM for 0.1 min, staying at 100 mM for 6.9 min, decreasing to 10 mM for 0.1 min, and maintaining at 10 mM for the last 4.9 min. The total analyzing time was 30 min. The flow rate was 0.25 mL/min and the injection volume was 50 μL . Retention times were 9.6 min for chloride and 7.9 min for bromate. LOQ were \sim 0.02 μM for chloride and \sim 0.01 μM for bromate.

Text S11. Ozonation experiment

Ozone stock solutions were prepared by sparging ozone-containing oxygen gas in ultrapure water cooled with ice. The ozone/oxygen gas mixture was produced by an ozone generator (BMT 803 BT, BMT Messtechnik, Berlin) fed with > 99.995% oxygen. Ozone concentrations in the stock solution were typically 1.6 – 1.8 mM determined by UV absorbance ($\epsilon_{260\text{nm}} = 3200 \text{ M}^{-1} \text{ cm}^{-1}$).²¹

Text S12. Quantum chemical calculation methods

The aqueous-phase free energy of formation, G_{aq} , of all species was obtained based on equation S9:

$$G_{\text{aq}} = \Delta G_{\text{solv,calc}} + G_{\text{corr,gas}} + E_{0,\text{gas}} \quad \text{Eq. S9}$$

$\Delta G_{\text{solv,calc}}$ is the solvation free energy of the species calculated using an implicit solvation model (SMD)²² in the absence or presence of explicit water molecules. $G_{\text{corr,gas}}$ is the gaseous phase correction to the free energy of the species solvated by explicit water molecules if explicit water molecules are

present. $E_{0,\text{gas}}$ is the electronic energy of the species solvated by explicit water molecules. The $\Delta G_{\text{solv,calc}}$ and $G_{\text{corr,gas}}$ values were calculated at the level of M06-2X/Aug-cc-pVDZ.²³ In particular, the $\Delta G_{\text{solv,calc}}$ values were calculated following the procedure of a continuum solvation method.²⁴ The $E_{0,\text{gas}}$ value was calculated at the level of M06-2X/Aug-cc-pVTZ.

Text S13. Validation of quantum chemical calculation methods

Theoretically calculated $\Delta G_{\text{solv,calc}}$ in the absence and presence of explicit water molecules ($n=1-3$) of Br^{\bullet} and Br^{-} were validated with experimentally measured or derived values. In the validation process, we included other halogen radicals and halides (i.e., F, Cl and I). Table S4 summarizes the theoretically calculated $\Delta G_{\text{solv,calc}}$ values and experimental values of halides and halogen radicals. The experimentally derived values of $\Delta G_{\text{solv,calc}}$ for halogen radicals (X^{\bullet} , where X is Cl or Br) were determined by the equation below²⁵ where IE(gas) and IE(aq) are the adiabatic gaseous and aqueous-phase ionization energy of X, respectively.

$$\Delta G_{\text{solv,calc}}(\text{X}^{\bullet}) = -\text{IE}(\text{gas}) + \Delta G_{\text{solv,calc}}(\text{X}^{-}) + \text{IE}(\text{aq}) \quad \text{Eq. S10}$$

The use of the hybrid DFT method, M06-2X, by validating the experimental one electron reduction potential of $\text{Br}^{\bullet}/\text{Br}^{-}$ by other quantum mechanical methods including CCSD(T)²⁶ and CBS-QB3^{27,28} and MP2 as summarized in Table S5. In addition to the validation of the one electron reduction potential for $\text{Br}^{\bullet}/\text{Br}^{-}$, one the electron reduction potentials for benzene, toluene, and anisole are validated Table S6.

Text S14. Calculation of free energy of activation by the Marcus theory

Based on the validation, we used the G_{aq} values obtained at the level of M06-2X/Aug-cc-pVDZ//M06-2X/Aug-cc-pVTZ with 3 explicit water molecules. We used Spartan 18 (Wavefunction, Irvine, CA)²⁹ to search the conformers of an adduct comprised of Br^{\bullet} and a target organic compound using a modified MMFF method.³⁰ The aqueous-phase free energy of adduct formation, $\Delta G_{\text{aq,calc}}^{\text{adduct}}$, was calculated as below:

$$\Delta G_{\text{aq,calc}}^{\text{adduct}} = G_{\text{adduct,aq}} - (G_{\text{R,aq}} + G_{\text{Br}^{\bullet},\text{aq}}) \quad \text{Eq. S11}$$

where $G_{\text{adduct,aq}}$, $G_{\text{R,aq}}$, and $G_{\text{Br}^{\bullet},\text{aq}}$ are the aqueous-phase free energies of formation of an adduct, of the target compound, R, and Br^{\bullet} , respectively.

The single electron transfer (SET) reaction of Br[•] with an organic compound is not a barrierless interior reaction. Thus, we used the Marcus theory³¹ to calculate the aqueous phase free energy of activation, $\Delta G_{\text{aq,SET}}^{\text{act}}$, in equation as no bond cleavage is involved in the SET reaction of Br[•] (i.e., dissociative electron transfer).

$$\Delta G_{\text{aq,SET}}^{\text{act}} = (1 + \Delta G_{\text{aq,SET}}^{\text{react}})^2 / 4\lambda \quad \text{Eq. S12}$$

Where $\Delta G_{\text{aq,SET}}^{\text{react}}$ is the standard state aqueous phase free energy of reaction, kcal/mol. The reorganization energy, λ , has two components: (1) the inner-sphere part that represents the change in the structure of solute and (2) the outer-sphere part that represents the change in the structure of the surrounding solvent. The λ_{in} values were calculated as:

$$\lambda_{\text{in}} = \Delta E_{\text{aq,SET}}^{\text{react}} - \Delta G_{\text{aq,SET}}^{\text{react}} \quad \text{Eq. S13}$$

$$\Delta E_{\text{aq,SET}}^{\text{react}} = \Delta E_{\text{aq,vertical}}^{\text{react}} - \Delta E_{\text{aq,reactants}}^{\text{react}} \quad \text{Eq. S14}$$

where $\Delta E_{\text{aq,SET}}^{\text{react}}$ is the standard state aqueous phase reaction energy change between reactants and products, $\Delta E_{\text{aq,vertical}}^{\text{react}}$ is the standard state energy change for vertical product and $\Delta E_{\text{aq,reactants}}^{\text{react}}$ is the standard state energy of reactants. We calculated the λ_{out} values based on the two-sphere model in a continuum medium proposed by Marcus:³¹

$$\lambda_{\text{out}} = \Delta e^2 N_{\text{A}} \left(\frac{1}{2r_1} + \frac{1}{2r_2} - \frac{1}{R} \right) \left(\frac{1}{\epsilon_0} - \frac{1}{\epsilon_s} \right) \quad \text{Eq. S15}$$

where Δe is the amount of charge transferred, N_{A} is the Avogadro's number; r_1 and r_2 are the ionic radii of the reactant molecules 1 and 2, respectively, and $R = r_1 + r_2$, ϵ_0 and ϵ_s are the optic (i.e., 78.39) and static (i.e., 1.77) dielectric constants of water, respectively, at 25 °C. Upon the calculations of the chloramine and the reaction product, radical cation, we used the λ_{out} obtained by treating the first solvation sphere explicitly with three water molecules. This way, the term λ_{in} also accounted for the outer-sphere reorganization of the first sphere in going from Br[•] to Br⁻, since the solvation pattern is different in these two species.

The calculated results for the organic model compounds and NH₂Cl are summarized in Table S8.

Text S15. LC-HRMS/MS evidences supporting the formation of C₆H₃BrO₃ and C₆H₅BrO₃ for the phenol-Br[•] reaction

Based on the LC-HRMS/MS analyses of the γ -radiolysis of phenol, two suspected products were detected containing Br (C₆H₃BrO₃ and C₆H₅BrO₃) with masses of 200.9193 and 202.9349 as [M-H]⁻

corresponding to $C_6H_3^{79}BrO_3$ and $C_6H_5^{79}BrO_3$, respectively, with mass deviation < 1 ppm (Figure S11, Table S3). The presence of Br in the suggested molecular formulas was confirmed by the detection of the ^{81}Br isotopes with similar peak height, corresponding to the natural abundance of the Br isotope of $^{79}Br:^{81}Br = 1:0.97$. Neither of them appeared in blank samples, but showed a gradual increase over time during γ -radiolysis experiments (Figure S12). Based on the molecular formula, *p*-benzoquinone substituted by a hydroxy group and a Br was suggested as a possible molecular structure for $C_6H_3BrO_3$ (Scheme 1, main text). To confirm this, the substituted *p*-benzoquinone was synthesized by brominating 1,2,4-benzenetriol by *N*-bromosuccinimide and subsequently oxidizing the hydroxy groups by the Fétizon's reagent (Ag_2CO_3 on celite) to a quinone group. The synthesized product was analyzed by the same LC-HRMS/MS method and its MS spectrum was compared to those obtained from the γ -radiolysis samples containing phenol. The same mass was observed in the synthesized chemical and in the γ -radiolysis sample, with a similar MS^2 spectral pattern, but at a different retention time (difference of 4.1 min, Figure S13). This indicates that the synthesized chemical is likely an isomer of the suspected product formed during the γ -radiolysis. The masses corresponding to $C_6H_3BrO_3$ and $C_6H_5BrO_3$ were also detected in the γ -radiolysis sample containing *p*-benzoquinone (instead of phenol) as a starting compound, showing a similar formation trend (Figure S12). This additionally supports that $C_6H_3BrO_3$ and $C_6H_5BrO_3$ are likely to have a quinone structure.

Text S16. Formation pathway of 4-bromophenol from the phenol- Br^\bullet reaction

A minor pathway of the reaction of phenol with Br^\bullet leads to the formation of 4-bromophenol with 4% yield (Scheme 1, main text). This implies a possible addition mechanism where a bromo-hydroxycyclohexadienyl radical formed by the addition of Br^\bullet to phenol is oxidized to a monobromophenol by any oxidant available in reaction solution, such as *p*-benzoquinone (Scheme S1(3)). This would be comparable to the formation of quinones from dihydroxycyclohexadienyl radicals observed for the oxidation of phenol by $^\bullet OH$.³² Alternatively, 4-bromophenol can be also formed from PhO^\bullet by a radical-radical coupling of PhO^\bullet and Br^\bullet . The ΔG_{aq}^{react} of PhO^\bullet with Br^\bullet for all possible resonance structures of PhO^\bullet (Figure S17) were calculated as -28.1 and -31.1 kcal/mol for the formation of 2-bromophenol and 4-bromophenol, respectively, and 6.3 kcal/mol of ΔG_{aq}^{act} . The coupling reaction on both *ortho*- and *para*-positions of PhO^\bullet are similarly favorable according to the calculated ΔG_{aq}^{react} , which however disagrees with the experimental result where only 4-bromophenol was detected. The dominance of the *para*-product is different from the reaction of phenol with HOBr, for which the *ortho*- and *para*-positions are similarly susceptible.^{33,34} The distinction may come from the different nature of the PhO^\bullet - Br^\bullet reaction

mechanism (radical-radical coupling) compared to phenol-HOBr (electrophilic aromatic substitution),³³ but more information is needed to clarify this.

Text S17. Principles of the chlorine-ammonia pretreatment as a bromate mitigation strategy of ozonation

The chlorine-ammonia pretreatment is a proven strategy to mitigate bromate during ozonation.²¹ It was originally designed to pre-oxidize bromide to HOBr, which can then be quenched by addition of ammonium.^{35,36} The formed monobromamine reacts moderately with ozone to bromide and nitrate.³⁷ Furthermore, the residual chlorine also reacts with ammonia to NH₂Cl. NH₂Cl has an additional benefit, because it also scavenges •OH ($k_{\bullet\text{OH},\text{NH}_2\text{Cl}} = 5.2 \times 10^8 \text{ M}^{-1} \text{ s}^{-1}$ or $5.7 \times 10^8 \text{ M}^{-1} \text{ s}^{-1}$).^{38,39} Overall, the chlorine-ammonia process blocks the initial steps for bromate formation by: (1) masking bromide and preventing it from being oxidized to HOBr by ozone and to Br• by •OH (i.e., blocking reactions 1 and 2, main text) and (2) scavenging •OH.

Text S18. Calculation of the fractions of Br•-related reactions during ozonation

Ozone, DOM, and Br⁻ are considered the main Br• consumers during ozonation. They produce bromine monoxide (BrO•, a transient species in bromate formation during ozonation),¹⁰ DOM oxidation products (e.g., quinones (section 3.2 in the main text), and Br₂•⁻, respectively, as a result of the reaction with Br•. In addition, a Br•-specific quencher such as NH₂Cl tested in this study consumes Br• as well. The fraction of Br• reacting with each consumer (e.g., f(Br•+NH₂Cl) for the fraction reacting with NH₂Cl) was calculated (Eqs. S16 – S18). The calculated f(Br•+X) as a function of varying conditions are shown in Figure 3 (main text) and in Figures S18 and S19.

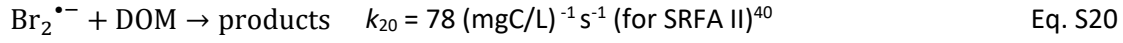
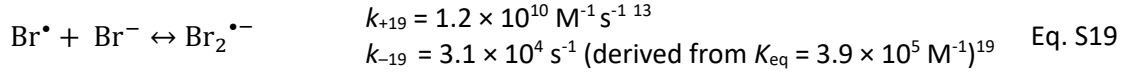
$$-\frac{d[\text{Br}^\bullet]}{dt} = k_{\text{Br}^\bullet, \text{O}_3} [\text{Br}^\bullet][\text{O}_3] + k_{\text{Br}^\bullet, \text{DOM}} [\text{Br}^\bullet][\text{DOM}] + k_{\text{Br}^\bullet, \text{Br}^-} [\text{Br}^\bullet][\text{Br}^-] + k_{\text{Br}^\bullet, \text{NH}_2\text{Cl}} [\text{Br}^\bullet][\text{NH}_2\text{Cl}] \quad \text{Eq. S16}$$

$$-\frac{d[\text{Br}^\bullet]}{[\text{Br}^\bullet]} = (k_{\text{Br}^\bullet, \text{O}_3} [\text{O}_3] + k_{\text{Br}^\bullet, \text{DOM}} [\text{DOM}] + k_{\text{Br}^\bullet, \text{Br}^-} [\text{Br}^-] + k_{\text{Br}^\bullet, \text{NH}_2\text{Cl}} [\text{NH}_2\text{Cl}]) dt \quad \text{Eq. S17}$$

$$f(\text{Br}^\bullet + \text{NH}_2\text{Cl}) = \frac{k_{\text{Br}^\bullet, \text{NH}_2\text{Cl}} [\text{NH}_2\text{Cl}]}{(k_{\text{Br}^\bullet, \text{O}_3} [\text{O}_3] + k_{\text{Br}^\bullet, \text{DOM}} [\text{DOM}] + k_{\text{Br}^\bullet, \text{Br}^-} [\text{Br}^-] + k_{\text{Br}^\bullet, \text{NH}_2\text{Cl}} [\text{NH}_2\text{Cl}])} \quad \text{Eq. S18}$$

The selected k_{Br^\bullet} for the f(Br•+X) calculation were $1.5 \times 10^8 \text{ M}^{-1} \text{ s}^{-1}$ for ozone,¹⁰ $1.7 \times 10^4 (\text{mgC/L})^{-1} \text{ s}^{-1}$ for DOM (Table 1, main text), $4.2 \times 10^7 \text{ M}^{-1} \text{ s}^{-1}$ for Br⁻ (see below), and $4.4 \times 10^9 \text{ M}^{-1} \text{ s}^{-1}$ for NH₂Cl (Table 1, main text). The k_{Br^\bullet} of $4.2 \times 10^7 \text{ M}^{-1} \text{ s}^{-1}$ for Br⁻ is an apparent k_{Br^\bullet} calculated by taking into account the

reverse reaction of Br^\bullet and Br^- (Eq. S19) and a subsequent reaction of $\text{Br}_2^{\bullet-}$ with DOM (Eq. S20) for $[\text{DOM}] = 1.4 \text{ mgC/L}$. Details on deriving the apparent k_{Br^\bullet} are shown below.



According to the Eqs. S19 and S20, the rate expression for Br^\bullet and $\text{Br}_2^{\bullet-}$ are as follows:

$$-\frac{d[\text{Br}^\bullet]}{dt} = k_{+19}[\text{Br}^\bullet][\text{Br}^-] - k_{-19}[\text{Br}_2^{\bullet-}] \quad \text{Eq. S21}$$

$$-\frac{d[\text{Br}_2^{\bullet-}]}{dt} = k_{20}[\text{Br}_2^{\bullet-}][\text{DOM}] + k_{-19}[\text{Br}_2^{\bullet-}] - k_{+19}[\text{Br}^\bullet][\text{Br}^-] \quad \text{Eq. S22}$$

Assuming $\text{Br}_2^{\bullet-}$ is in steady-state, Eq. S22 can be expressed in terms of the concentration of $\text{Br}_2^{\bullet-}$:

$$[\text{Br}_2^{\bullet-}]_{ss} = \frac{k_{+19}[\text{Br}^\bullet][\text{Br}^-]}{(k_{20}[\text{DOM}] + k_{-19})} \quad \text{Eq. S23}$$

By substituting Eq. S21 with Eq. S23, the rate expression for Br^\bullet is converted to Eq. S24 and finally k_{app} is obtained as a value dependent on DOM concentration (e.g., $k_{\text{app}} = 4.2 \times 10^7 \text{ M}^{-1} \text{ s}^{-1}$ for 1.4 mgC/L DOM).

$$-\frac{d[\text{Br}^\bullet]}{dt} = \frac{k_{+19}k_{20}[\text{DOM}]}{(k_{20}[\text{DOM}] + k_{-19})} [\text{Br}^\bullet][\text{Br}^-] = k_{\text{app}}[\text{Br}^\bullet][\text{Br}^-] \quad \text{Eq. S24}$$

Table S1. Chemical reagents

Compound	Supplier	Catalog no.	Purity
1,2-Dibromoethane	Sigma-Aldrich	240656	≥ 99%
2,2'-Azino-bis(3-ethylbenzothiazoline-6-sulfonic acid) diammonium salt (ABTS)	Sigma-Aldrich	10102946001	> 98%
3-Phenylpropionic acid	Alfa Aesar	A14908	99%
4-Chlorobenzoic acid	Sigma-Aldrich	135585	99%
4-Bromophenol	Fluk	18010	≥ 98%
4-chlorophenol	Riedel-de Haën	35826	99.8%
4-iodophenol	Fluka	58020	≥ 98%
Ammonium sulfate	Sigma-Aldrich	A5132	≥ 99%
Anisole	Sigma-Aldrich	123226	99%
Benzene	Sigma-Aldrich	32212	≥ 99%
Benzoic acid	Sigma-Aldrich	33047	≥ 99%
<i>p</i> -Benzoquinone	Sigma-Aldrich	B10358	≥ 98%
Benzylamine	Sigma-Aldrich	185701	99%
<i>N,N</i> -Dimethylbenzylamine	Sigma-Aldrich	185582	≥ 99%
Formic acid	Sigma-Aldrich	1.00264	90-100%
Ibuprofen	Sigma-Aldrich	I1892	≥ 98%
Naphthalene	Fluka	70211	≥ 99%
Phenol	Fluka	77610	≥ 99%
Sorbic acid	Fluka	85510	≥ 99%
Toluene	Merck	1.08325	≥ 99%
<i>trans</i> -cinnamic acid	Sigma-Aldrich	C80857	≥ 99%
<i>tert</i> -butanol	Sigma-Aldrich	19460	≥ 99%
Sodium hypochlorite solution	Sigma-Aldrich	13440	6-14% active chlorine
Suwannee River Humic Acid Standard II	IHSS	2S101F	52.34% carbon as dry, ash-free sample
Silver nitrate	Merck	1512	≥ 99%
Hydroquinone	Sigma-Aldrich	H9003	≥ 99%
Catechol	Merck	82261	≥ 99%

Table S2. Compounds analyzed by HPLC and LC-HRMS/MS and the corresponding analytical condition and LOQ.

Compounds	Column	Detection ¹	RT, min	LOQ, μM	Measuring range
Benzylamine	HILIC	200nm (Em) /270nm (Ex)	6.9	1.2	2 – 3 μM
<i>N,N</i> -Dimethylbenzylamine	HILIC	200nm (Em) /270nm (Ex)	8.0	0.6	2 – 3 μM
4-Bromophenol	C18	220nm or MS	10.4 (UV), 18.5 (MS)	0.3 (MS)	1 – 3 μM
4-Chlorophenol	C18	220nm	9.3	0.6	0.6 – 3 μM
4-Iodophenol	C18	220nm	11.8	0.6	0.7 – 3 μM
Anisole	C18	267nm	10.5	0.3	1 – 3 μM
Benzene	C18	200nm (Em) /270nm (Ex)	11.0	2.5	3 – 4 μM
Benzoic acid	C18	230nm	6.7	0.3	2 – 3 μM
<i>p</i> -Chlorobenzoic acid	C18	230nm	11.5	0.6	2 – 3 μM
Ibuprofen	C18	220nm	18.1	0.2	0.3 – 4 μM
Naphthalene	C18	220nm	16.9	0.2	0.2 – 2 μM
Phenol	C18	200nm (Em) /310nm (Ex)	5.1	0.2	2 – 3 μM
Toluene	C18	210nm	14.5	1.5	2 – 3 μM
3-Phenylpropionic acid	C18	210nm	7.8	0.3	2 – 3 μM
<i>p</i> -Benzoquinone	C18	254nm	3.0	0.6	0.8 – 4 μM
Sorbic acid	C18	267nm	6.6	0.2	0.3 – 3 μM
<i>trans</i> -Cinnamic acid	C18	267nm	9.3	0.1	1 – 3 μM
Hydroquinone	C18	220nm	5.6	0.6	0.1 – 0.6 μM
Catechol	C18	MS	8.4	0.02	0.02 – 0.1 μM

¹Diode-array detector, fluorescence detector, or mass spectrometer

Table S3. Detected exact masses and mass deviation by LC-HRMS/MS.

Compounds	Molecular formula (M)	Polarity, Adduct	Theoretical exact mass	Detected mass	Mass deviation, ppm
Phenol	C ₆ H ₆ O	pos, M+H	95.0491	95.0491	0.0
<i>p</i> -Benzoquinone	C ₆ H ₄ O ₂	pos, M+H	109.0284	109.0285	0.9
4-Bromophenol	C ₆ H ₅ ⁷⁹ BrO	neg, M-H	170.9451	170.9454	1.8
	C ₆ H ₅ ⁸¹ BrO		172.9431	172.9429	1.2
Catechol	C ₆ H ₆ O ₂	neg, M-H	109.0295	109.0299	3.7
C ₆ H ₃ BrO ₃ (suspected)	C ₆ H ₃ ⁷⁹ BrO ₃	neg, M-H	200.9193	200.9194	0.5
	C ₆ H ₃ ⁸¹ BrO ₃		202.9172	202.9174	1.0
C ₆ H ₅ BrO ₃ (suspected)	C ₆ H ₅ ⁷⁹ BrO ₃	neg, M-H	202.9349	202.9352	1.5
	C ₆ H ₅ ⁸¹ BrO ₃		204.9329	204.9328	0.5
C ₆ H ₄ O ₃ (suspected)	C ₆ H ₄ O ₃	neg, M-H	123.0088	123.0090	1.6
C ₆ H ₆ O ₃ (suspected)	C ₆ H ₆ O ₃	neg, M-H	125.0244	125.0246	1.6
C ₆ H ₆ O ₄ (suspected)	C ₆ H ₆ O ₄	neg, M-H	141.0193	141.0196	2.1

C ₁₂ H ₁₀ O ₂ (suspected)	C ₁₂ H ₁₀ O ₂	neg, M-H	185.0608	185.0609	0.5
--	--	----------	----------	----------	-----

Table S4. Theoretically calculated $\Delta G_{\text{solv,calc}}$ values and experimental values of halides and halogen radicals in kcal/mol. n is the number of explicit water molecule(s).

X ⁻ or X [•]	$\Delta G_{\text{solv,calc}}$ (n=0)	$\Delta G_{\text{solv,calc}}$ (n=1)	$\Delta G_{\text{solv,calc}}$ (n=2)	$\Delta G_{\text{solv,calc}}$ (n=3)	$\Delta G_{\text{solv,exp}}$
F ⁻	-86.9	-96.0	-99.2	-104.6	-104.3 ⁴¹
Cl ⁻	-65.1	-69.1	-69.3	-71.0	-75.5 ²⁵
Br ⁻	-53.3	-58.7	-60.1	-63.0	-66.3 ⁴²
I ⁻	-64.1	-66.8	-66.0	-67.7	-57.4 ⁴²
Cl [•]	0.1	-4.0	-3.7	-4.3	-4.3 ^a
Br [•]	-0.8	-3.4	-1.1	-1.4	0.11 ^a

^a experimentally derived value in Eq. S10.

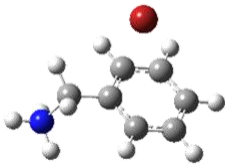
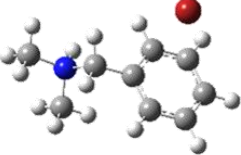
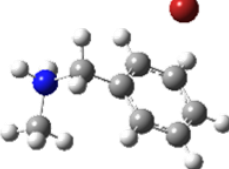
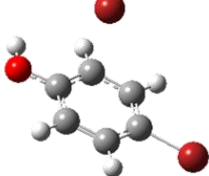
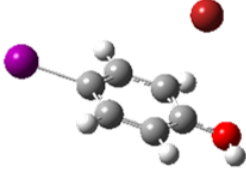
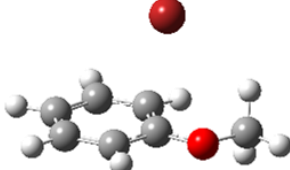
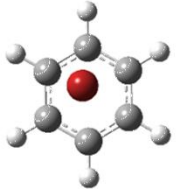
Table S5. Benchmark calculations of one electron reduction potential of Br[•]/Br⁻.

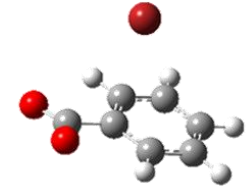
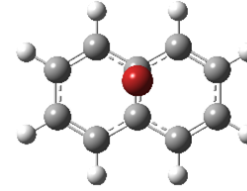
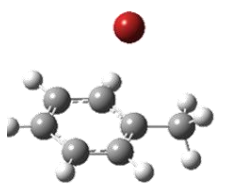
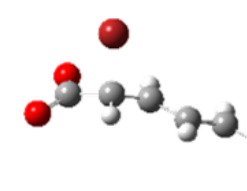
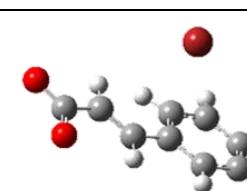
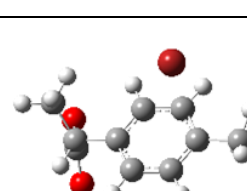
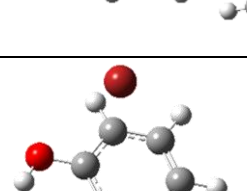
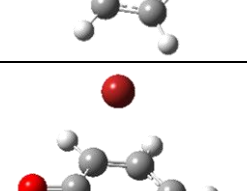
Method and basis set	E_{red}^0 , V
UCCSD(T)/Aug-cc-pVTZ	1.4
UCCSD(T)/Aug-cc-pVQZ	1.5
UCCSD(T)/Aug-cc-pV5Z	1.5
UCCSD(T)/Aug-cc-pVTZ	1.4
CBS-QB3//M06-2X/Aug-cc-pVDZ	1.5
MP2(FULL)/Aug-cc-pVDZ//M06-2X/Aug-cc-pVTZ	1.4
M06-2X/Aug-cc-pVDZ// M06-2X/Aug-cc-pVTZ (2 explicit water molecules)	1.7
M06-2X/Aug-cc-pVDZ// M06-2X/Aug-cc-pVTZ (3 explicit water molecules)	1.8
Experimental value ⁴³	1.8–2.2

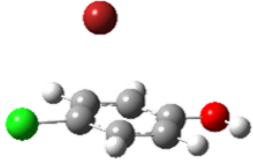
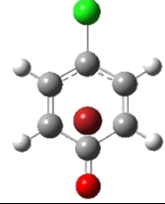

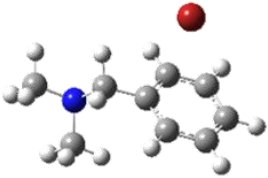
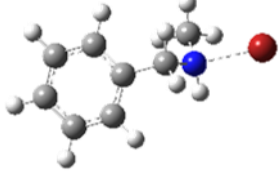
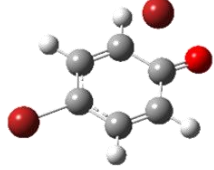
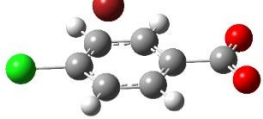
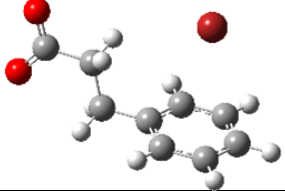
Table S6. Validation of one electron reduction potential for selected organic compounds at the M06-2X/Aug-cc-pVDZ//M06-2X/Aug-cc-pVTZ level of theory with the SMD solvation model

R/R ^{•+}	E_{red}^0 , V	Reference	$\Delta G_{\text{react,exp}}$, kcal/mol	$\Delta G_{\text{react,calc}}$, kcal/mol
C ₆ H ₆ / C ₆ H ₆ ^{•+}	-2.1	Pearson 1986 ⁴⁴	48.4	56.9
C ₆ H ₅ CH ₃ /C ₆ H ₅ CH ₃ ^{•+}	-1.98	Pearson 1986 ⁴⁴	45.7	49.1
C ₆ H ₅ OCH ₃ /C ₆ H ₅ OCH ₃ ^{•+}	-1.62	Jonsson et al. 1993 ⁴⁵	37.4	41.0

Table S7. Calculated free energy of adduct formation ($\Delta G^{\text{adduct}}_{\text{aq}}$) for the reactions of organic model compounds with Br^{\bullet} (red sphere) and the optimized molecular structures of the adducts.

No.	Compound	Optimized molecular structure of an adduct	$\Delta G^{\text{adduct}}_{\text{aq}}$, kcal/mol
1	Benzylamine		-0.4
2	<i>N,N</i> -Dimethylbenzylamine		-0.4
3	<i>N</i> -Methylbenzylamine		-0.3
4	4-Bromophenol		-0.8
5	4-Iodophenol		-1.4
6	Anisole		-2.5
7	Benzene		4.5

8	Benzoate		-0.6
9	Naphthalene		-0.6
10	Toluene		-1.4
11	Sorbic acid		-9.9
12	<i>trans</i> -Cinnamic acid		-1.3
13	Ibuprofen		-1.6
14	Phenol		-1.9
15	Phenolate		-19.8

16	4-Chlorophenol		-0.7
17	4-Chlorophenolate		-18.6
18	Benzylamine (deprotonated)		-8.4
19	<i>N,N</i> -Dimethylbenzylamine (deprotonated)		-12.2
20	<i>N</i> -Methylbenzylamine (deprotonated)		-10.8
21	4-Bromophenolate		-17.8
22	<i>p</i> -Chlorobenzoate		-0.6
23	3-Phenylpropionic acid		-1.2

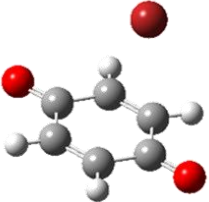
24	<i>p</i> -Benzoquinone	 A ball-and-stick model of p-benzoquinone. The molecule consists of a six-membered ring of carbon atoms (grey spheres) with two oxygen atoms (red spheres) attached to the ring at the para position. Each oxygen atom is double-bonded to a carbon atom in the ring. The ring is shown in a perspective view, with hydrogen atoms (white spheres) attached to the carbon atoms. The oxygen atoms are positioned at the top and bottom of the ring.	1.2
----	------------------------	--	-----

Table S8. Compiled QC calculation results for the reactions of the selected organic model compounds and of NH_2Cl with Br^- ($\Delta G^{\text{react}}_{\text{aq,calc}}$ as the standard state aqueous phase free energy of reaction, λ as the reorganization energy, and $\Delta G^{\text{act}}_{\text{aq,SET}}$ as the aqueous phase free energy of activation).

No.	Name	Structure	$\Delta G^{\text{react}}_{\text{aq,calc}}$ kcal/mol	λ , kcal/mol	$\Delta G^{\text{act}}_{\text{aq,SET}}$ kcal/mol
1	Benzylamine (protonated)		20.2	26.4	20.5
2	N,N- dimethylbenzylamine (protonated)		19.8	27.1	20.3
3	N-methylbenzylamine (protonated)		18.4	28.4	19.3
4	3,4-Chlorophenol		5.2	28.5	10.0
5	4-bromophenol		2.8	28.4	8.6
6	4-iodophenol		-3.4	27.3	5.3
7	Anisole		-0.5	28.0	6.7
8	Benzene		15.4	26.3	16.5
9	Benzoate		8.8	34.9	13.7
10	Naphthalene		-1.4	25.5	5.7
11	Toluene		7.6	26.9	11.1
12	Sorbic acid		-5.7	30.3	5.0
13	Trans-cinnamic acid		0.5	29.3	7.6
14	Ibuprofen		-23.9	63.7	6.2

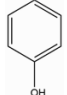
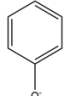

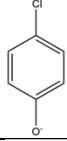
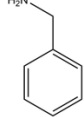
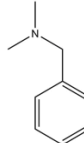
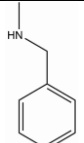
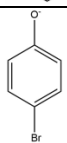
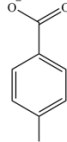
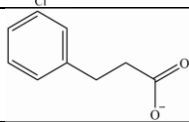
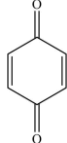
15	Phenol		0.9	28.0	7.5
16	Phenolate		-30.5	25.2	0.3
17	4-chlorophenol		1.5	28.5	7.9
18	4-chlorophenolate		-29.4	25.6	0.1
19	Benzylamine (deprotonated)		-1.9	36.0	8.1
20	N,N-dimethylbenzylamine (deprotonated)		-17.9	40.0	3.1
21	N-methylbenzylamine (deprotonated)		-10.4	36.3	4.6
22	4-bromophenolate		-28.5	25.9	0.1
23	p-chlorobenzoate		12.5	29.3	14.9
24	3-phenyl-propionate		4.5	37.8	11.8
25	p-benzoquinone		39.8	27.3	41.2
26	monochloramine	NH ₂ Cl	-34.0	65.5	3.8

Table S9. Spin density distribution of protonated and deprotonated forms of benzylamine and *N,N*-dimethylbenzylamine.

Perspective	Benzylamine (protonated)	Benzylamine (deprotonated)
A		
B		
Perspective	<i>N,N</i> -Dimethylbenzylamine (protonated)	<i>N,N</i> -dimethylbenzylamine (deprotonated)
A		
B		

Table S10. Scavenging rates (k_{species}' , s^{-1}) of e^- , $\cdot\text{OH}$, $\cdot\text{H}$, $\text{Br}\cdot$, and $\cdot\text{tBA}$ (*t*-butanol derived radical) by the reaction species in γ -radiolysis kinetic experiments (1,2-dibromoethane (1,2-DBE), Ag^+ , *t*-butanol, a model compound, phosphate ions ($\text{H}_2\text{PO}_4^-/\text{HPO}_4^{2-}$ for pH 7), and dissolved O_2), based on the reported or assumed second-order rate constants (k_{species} , $\text{M}^{-1}\text{s}^{-1}$) and the applied concentrations (conc., M).

species	conc.	k_{e^-}	k_{e^-}'	$k_{\cdot\text{OH}}$	$k_{\cdot\text{OH}}'$	$k_{\cdot\text{H}}$	$k_{\cdot\text{H}}'$	$k_{\text{Br}\cdot}$	$k_{\text{Br}\cdot}'$	$k_{\cdot\text{tBA}}$	$k_{\cdot\text{tBA}}'$
1,2-DBE	7.0×10^{-4}	1.4×10^{10} ¹²	9.8×10^6	2.4×10^8 ¹²	1.7×10^5	1.0×10^9 ^b	7.0×10^5	1.0×10^6 ⁴⁶	7.0×10^2	na	na
Ag^+	2.2×10^{-6}	3.7×10^{10} ⁴⁷	8.0×10^4	1.4×10^{10} ⁴⁷	3.0×10^4	2.0×10^{10} ⁴⁷	4.4×10^4	1.0×10^{10} ^b	2.2×10^4	1.0×10^9 ^b	2.2×10^3
<i>t</i> -butanol	4.0×10^{-3}	4.0×10^5 ⁴⁷	1.6×10^3	6.0×10^8 ⁴⁷	2.4×10^6	1.7×10^5 ⁴⁷	6.8×10^2	3.0×10^4 ^c	1.2×10^2	na	na
model ^a	3.4×10^{-6}	5.1×10^9 ⁴⁷	1.7×10^4	5.0×10^9 ⁴⁷	1.7×10^4	3.4×10^9 ⁴⁷	1.2×10^4	5.5×10^9 ^d	1.9×10^4	1.0×10^9 ^e	3.4×10^3
phosphate	5.0×10^{-2}	9.6×10^6 ⁴⁷	4.8×10^5	8.5×10^4 ⁴⁷	4.3×10^3	2.8×10^5 ⁴⁷	1.4×10^4	na	na	na	Na
O_2	6.8×10^{-5}	1.9×10^{10} ⁴⁷	1.3×10^6	na	na	na	na	na	na	1.0×10^9 ^b	6.8×10^4
total ^f			1.2×10^7		2.6×10^6		7.7×10^5		4.1×10^4		6.8×10^4

^a naphthalene as an example; ^b assumed; ^c average value of ¹³ and ¹⁴; ^d Table 1 (main text); ^e assumed based on the reaction of $\cdot\text{tBA}$ with histidine¹⁷; ^f total calculated scavenging rate as a sum of the scavenging rates of all species

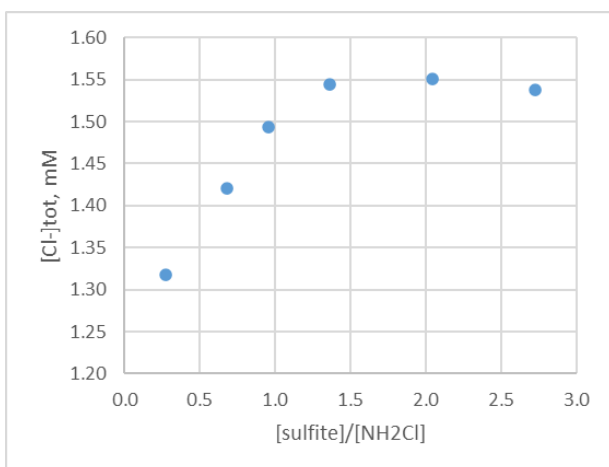


Figure S1. Total chloride concentrations ($[\text{Cl}^-]_{\text{tot}}$) of primary NH_2Cl stock solutions after reducing NH_2Cl by sulfite. $[\text{Cl}^-]_{\text{tot}}$ indicates the sum of the chloride concentration already present in the stock solution and chloride formed from the reduction of NH_2Cl with sulfite. The NH_2Cl concentration of the stock solution was 0.38 mM.

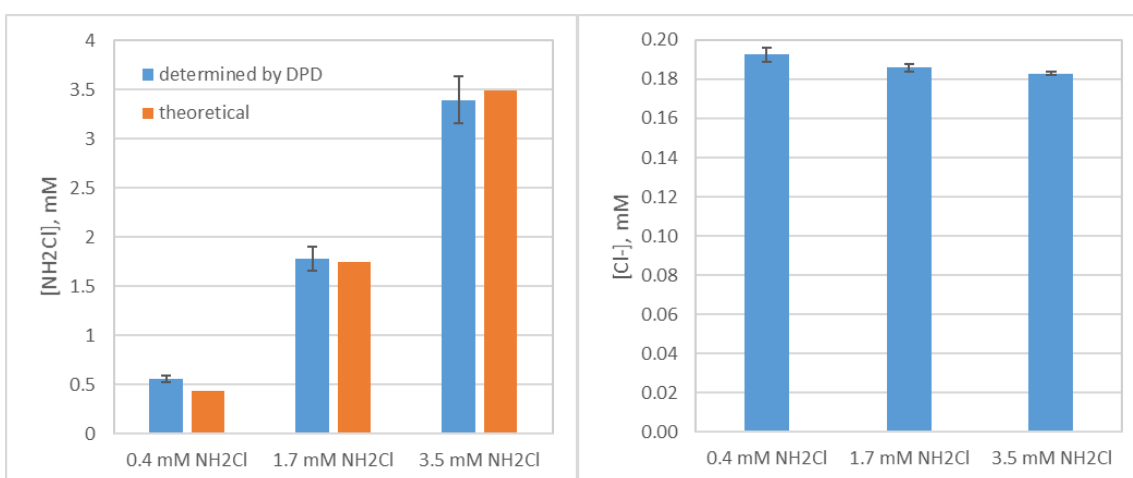


Figure S2. Left: Determined and theoretical NH_2Cl concentrations in supernatant of the silver(I)-treated NH_2Cl stock solutions (as 0.4mM, 1.7mM and 3.5mM NH_2Cl); right: measured chloride concentrations in 0.2 mM NH_2Cl solutions prepared by diluting 0.4, 1.7, or 3.5 mM NH_2Cl stock solutions and reducing NH_2Cl of each solution by sulfite.

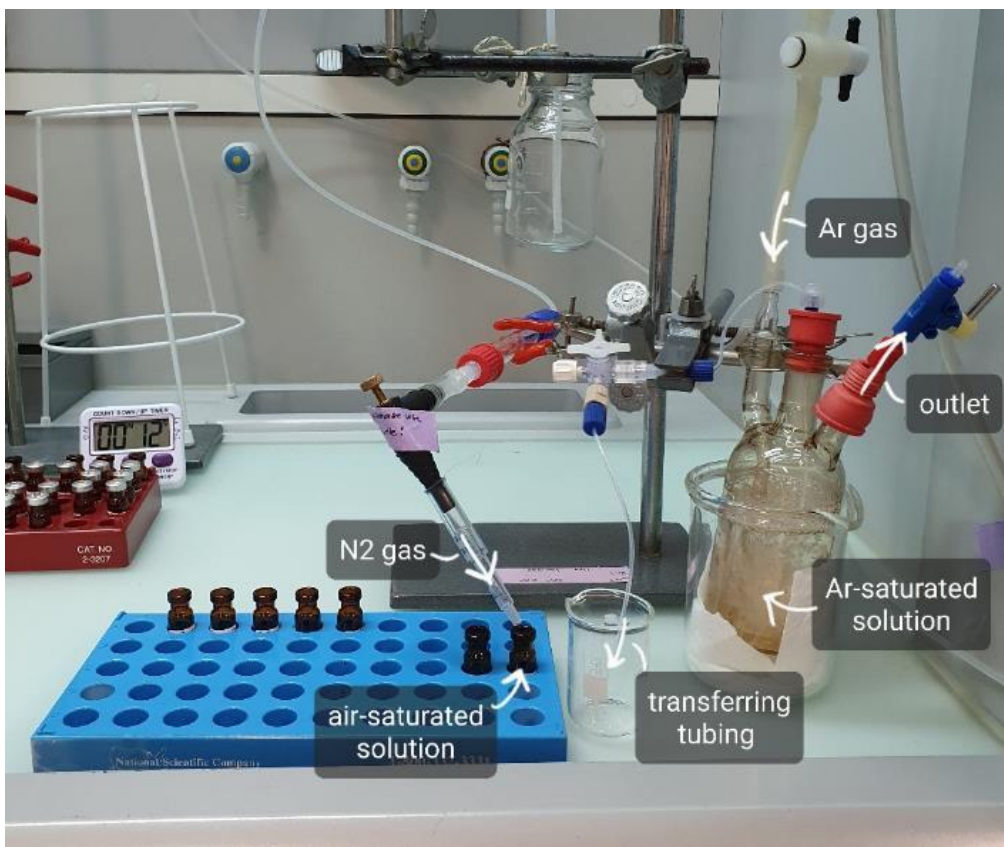


Figure S3. Setup for preparing γ -radiolysis samples for the competition kinetics experiments. To transfer the Ar-saturated solution to the sample vials containing an air-saturated solution (shown as 1.5mL amber vials with crimp neck), the transferring tubing was placed to the bottom of the vials.

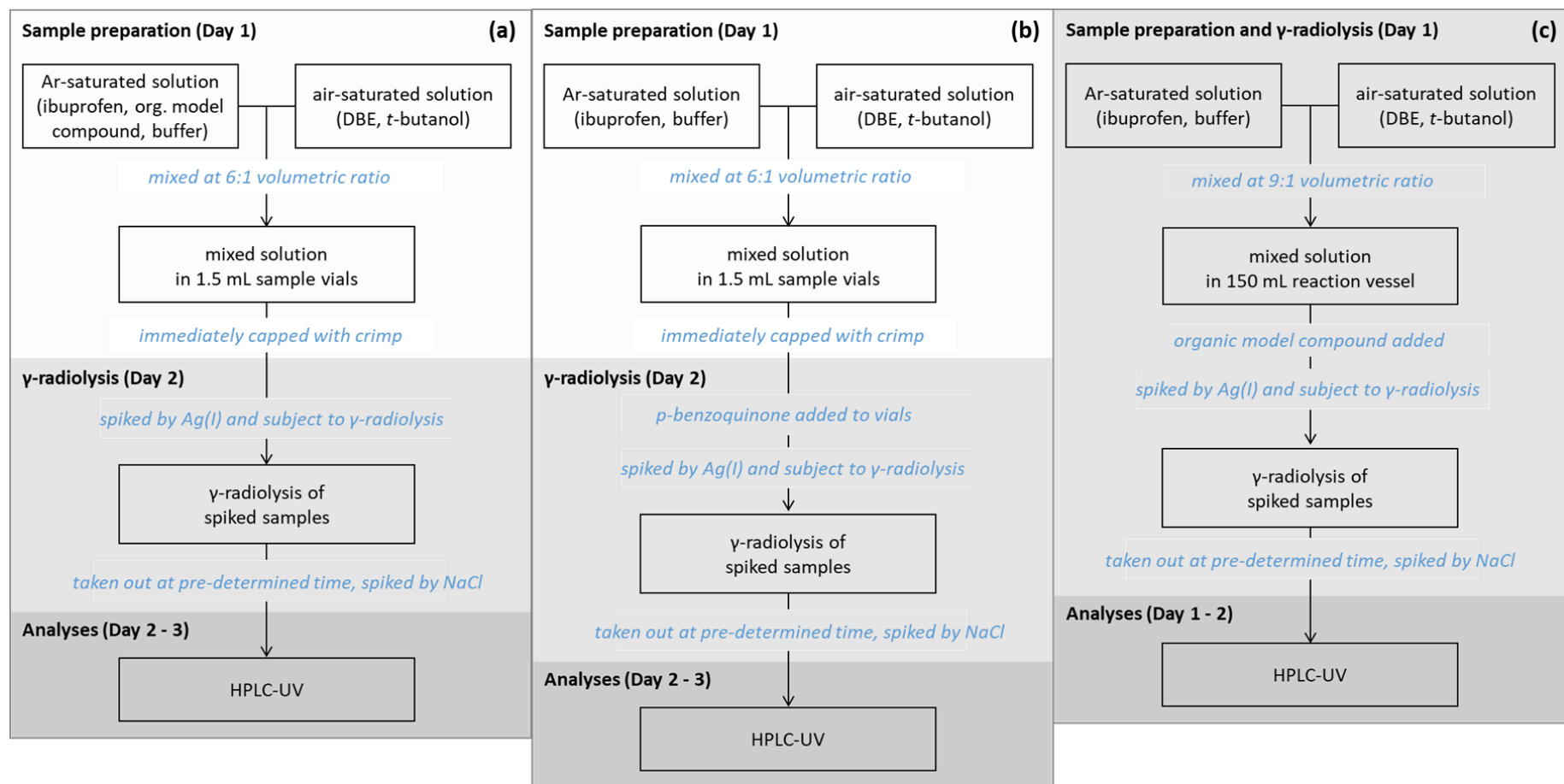
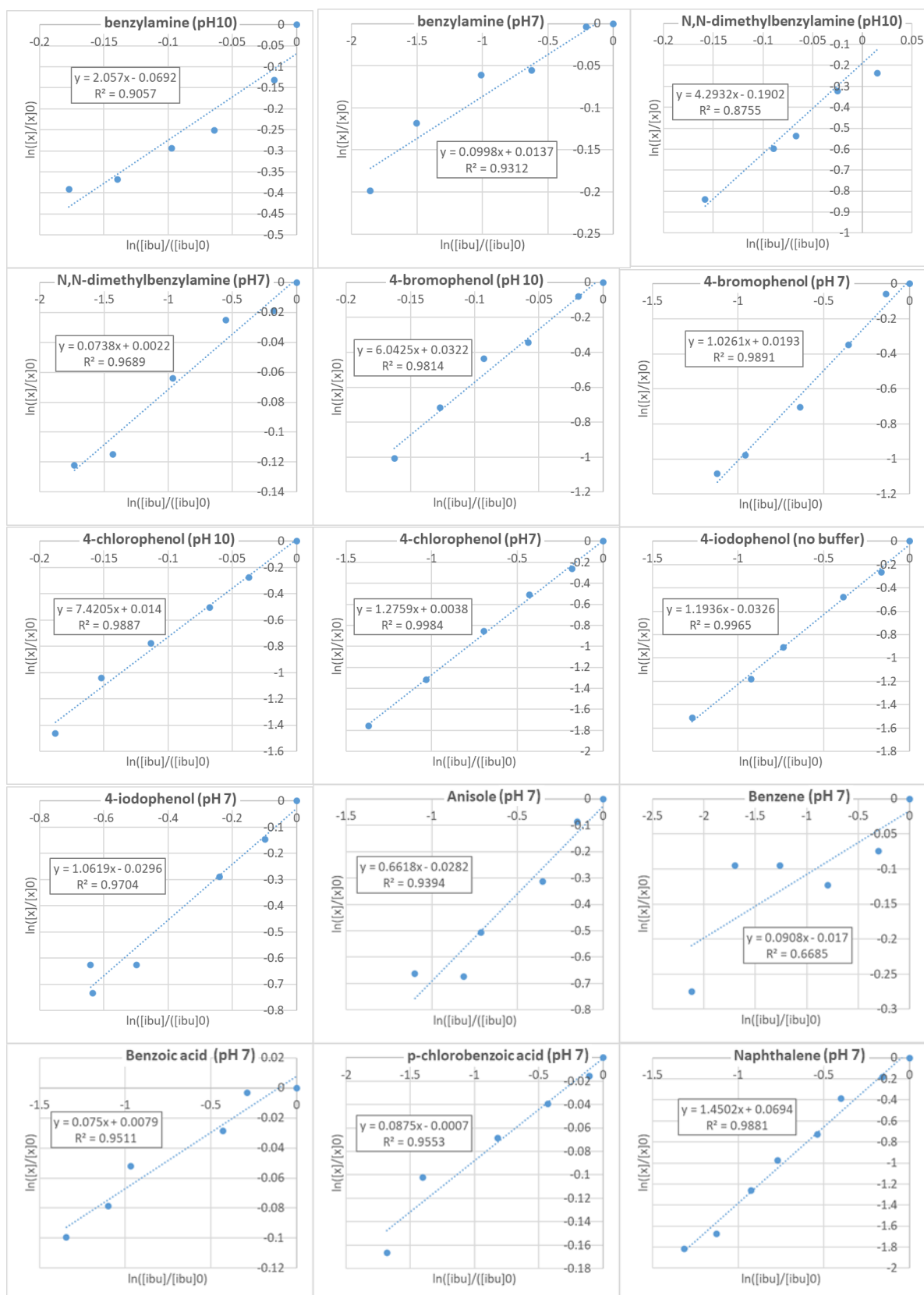
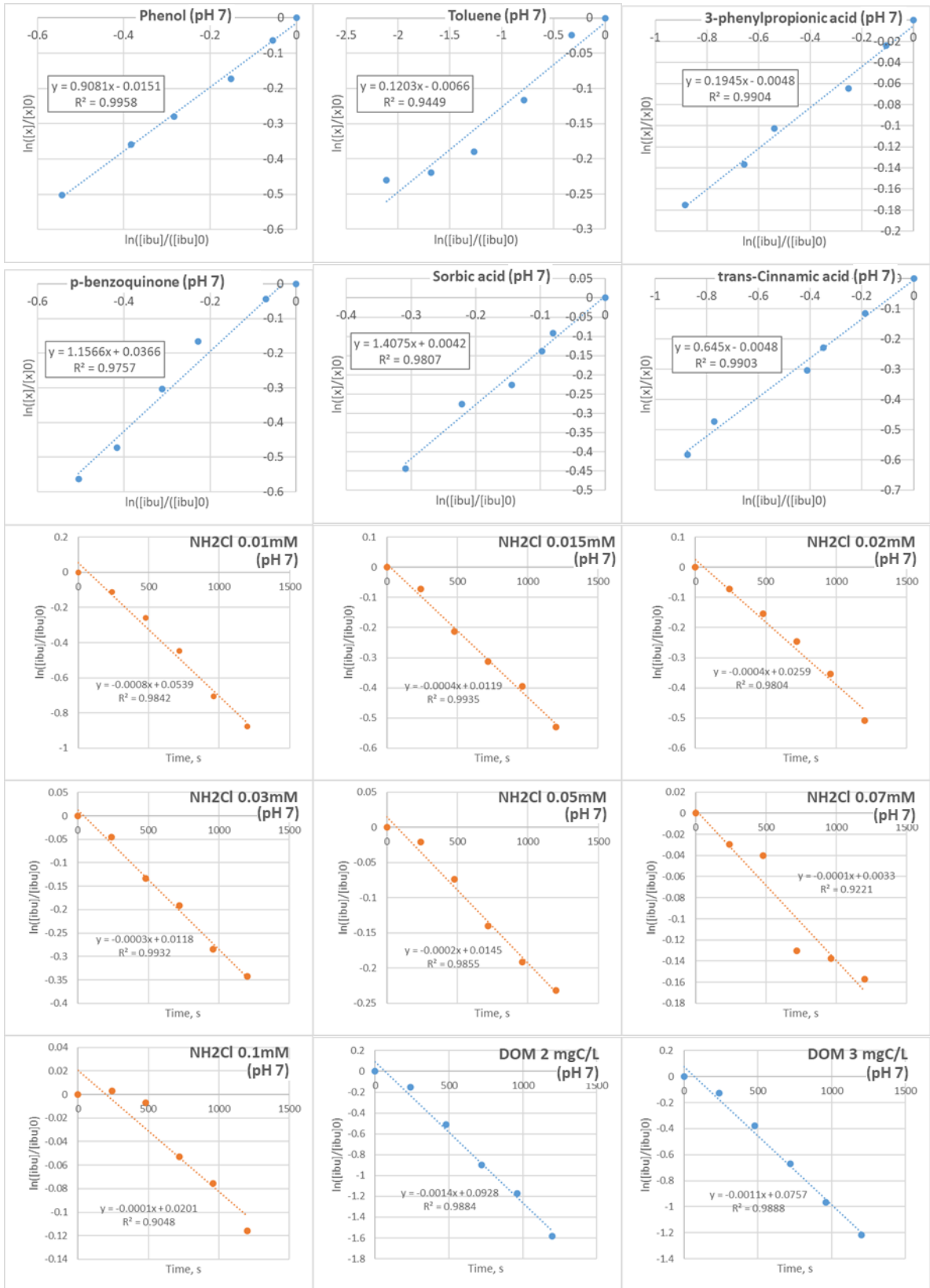


Figure S4. Flow charts of the sample preparation for kinetic experiments performed with γ -radiolysis for (a) most organic model compounds, (b) *p*-benzoquinone, and (c) benzene, toluene, and naphthalene. DBE stands for 1,2-dibromoethane. Background shades separate the days on which an individual step (preparation, γ -radiolysis, and analyses) was carried out.





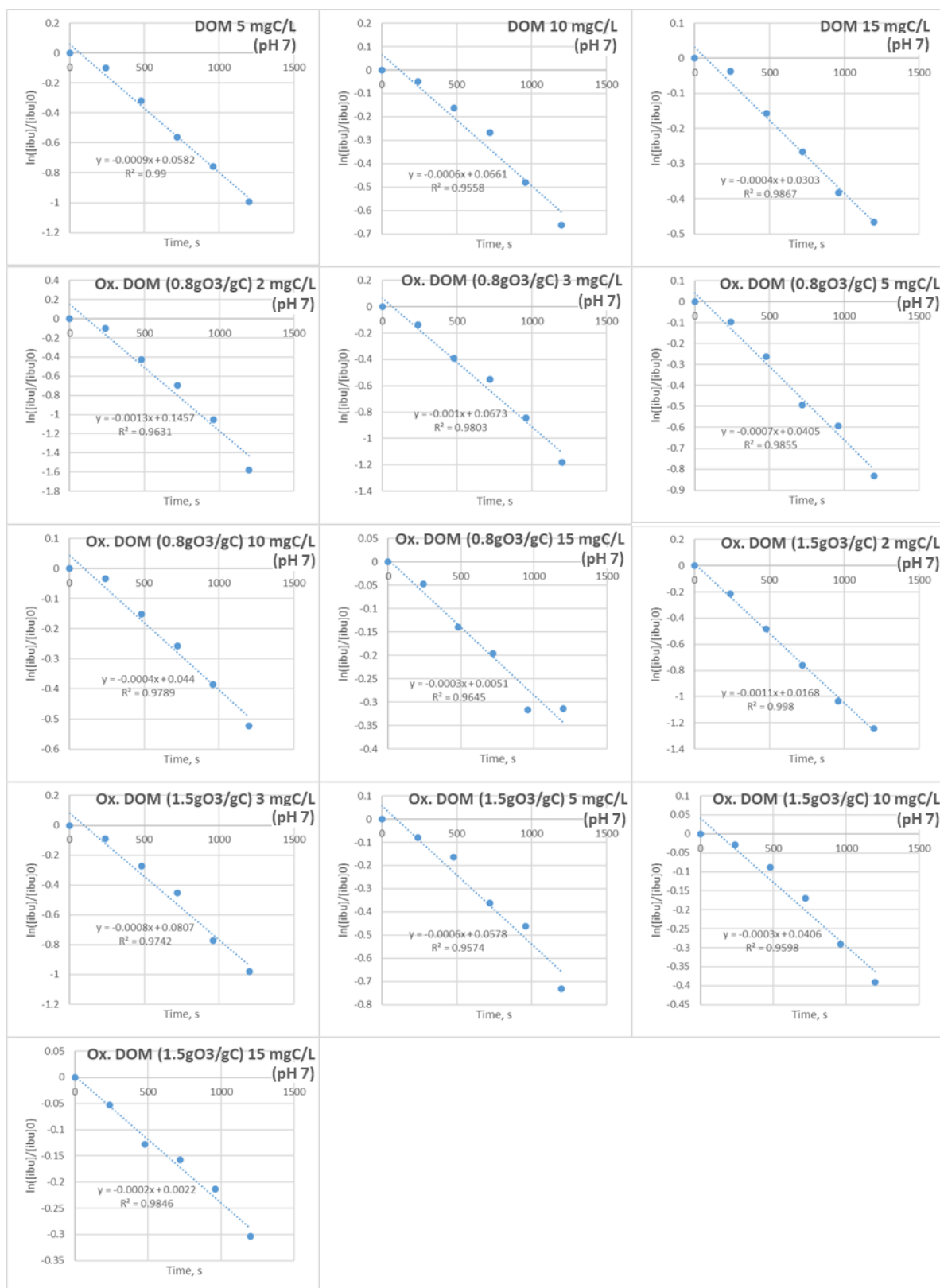


Figure S5. Competition kinetics plots for the reactions of Br^\bullet with the organic model compounds, NH_2Cl , DOM, and oxidized DOM (by 0.8 gO_3/gC or 1.5 gO_3/gC) at pHs 7.1 or 10.2. Concentrations of the model compounds were fixed at 3.0 – 3.4 μM . Concentrations of NH_2Cl , DOM, and oxidized DOM are stated in the figure headings. Data points are from a single measurement and k_{Br^\bullet} was calculated mostly based on an average of experimental duplicates.

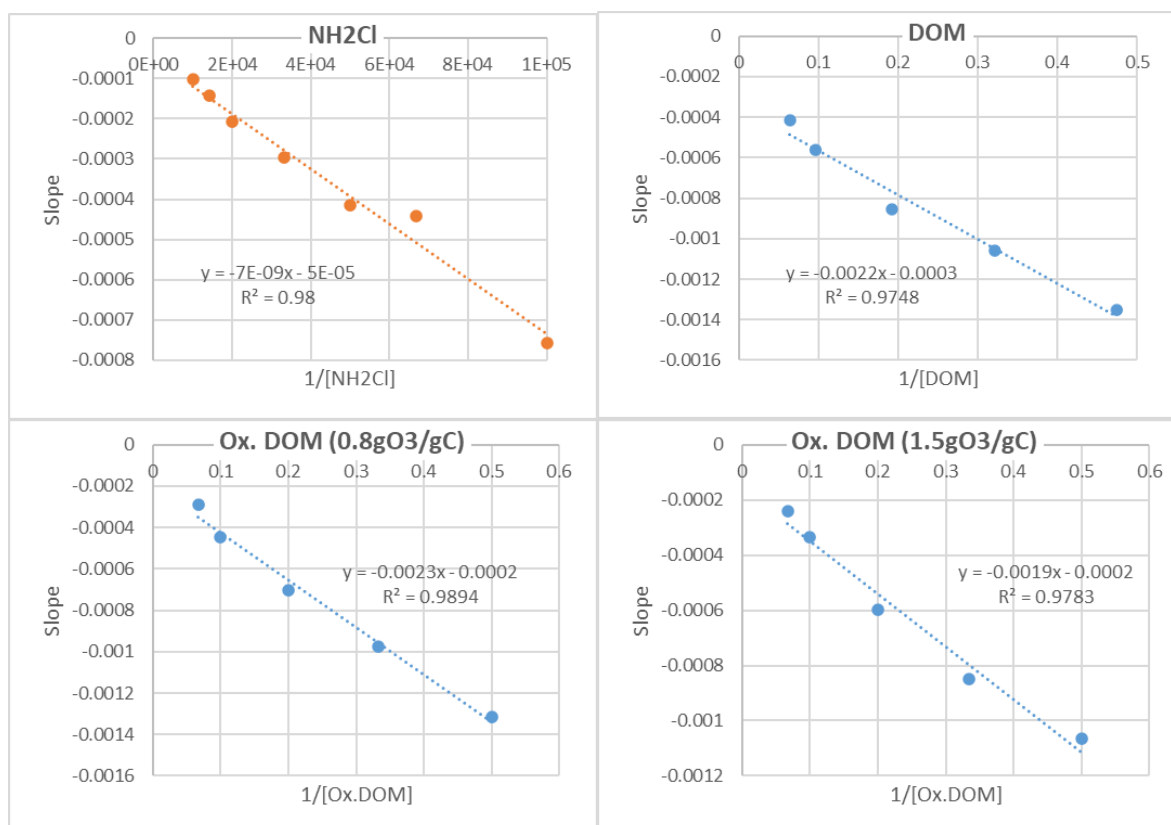


Figure S6. Slopes obtained by linear regression of data points of the competition kinetics plots (shown in Figure S5) as a function of a reciprocal of the DOC or NH₂Cl concentration, to derive $k_{Br\cdot}$ for NH₂Cl, DOM, and oxidized DOM (by 0.8 gO₃/gC or 1.5 gO₃/gC). See Text S8 for the corresponding rate expression.

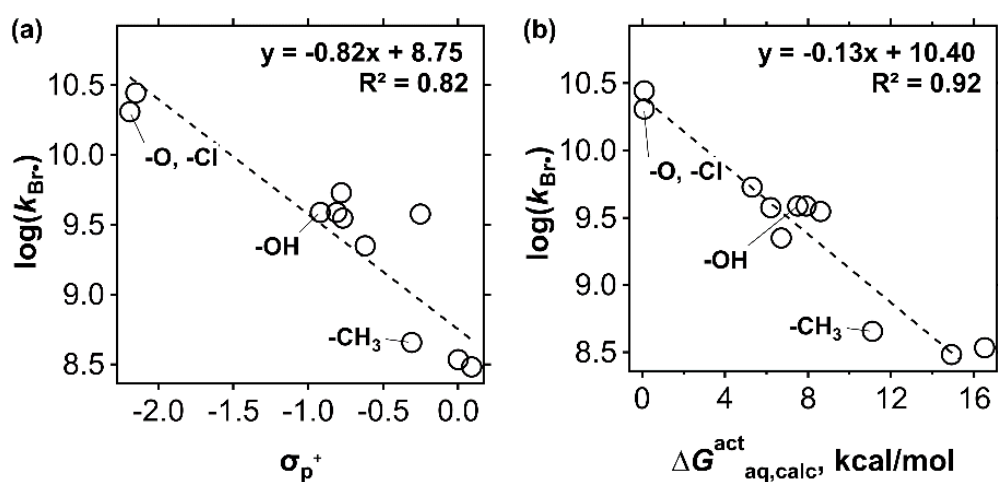


Figure S7. Quantitative structure-activity relationship of the measured $k_{Br\cdot}$ of the selected aromatic model compounds with (a) Hammett constants and (b) computed activation energies.

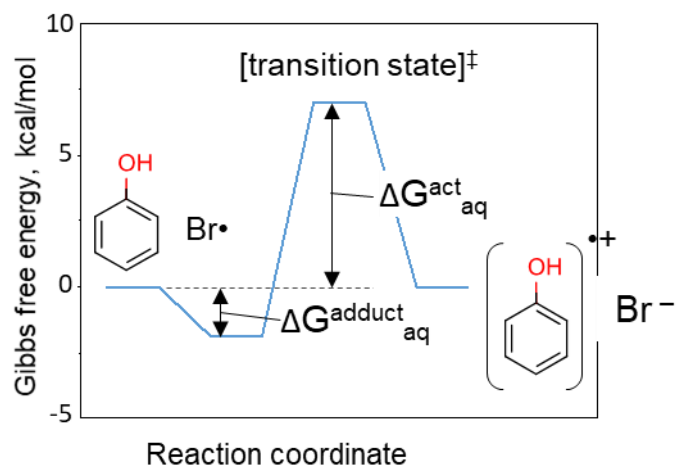


Figure S8. Schematic reaction coordinate for the reaction of phenol with Br^\bullet .

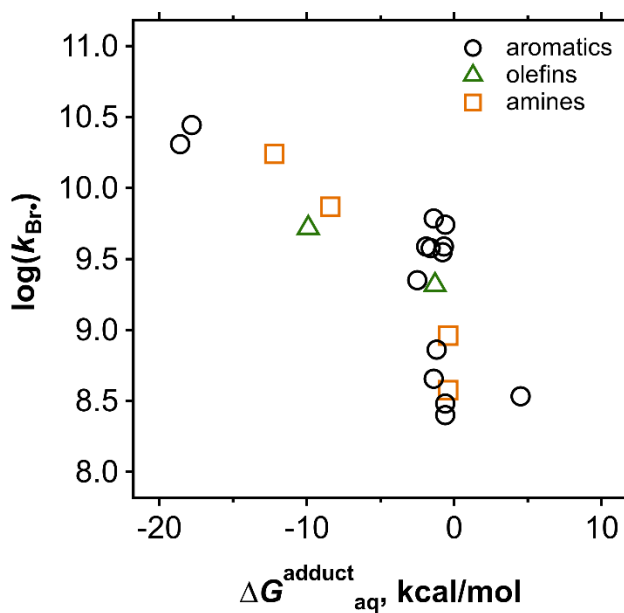


Figure S9. Correlation between the measured k_{Br^\bullet} of the selected organic model compounds and aqueous phase free energies for the formation of adducts ($\Delta G^{\text{adduct}}_{\text{aq}}$).

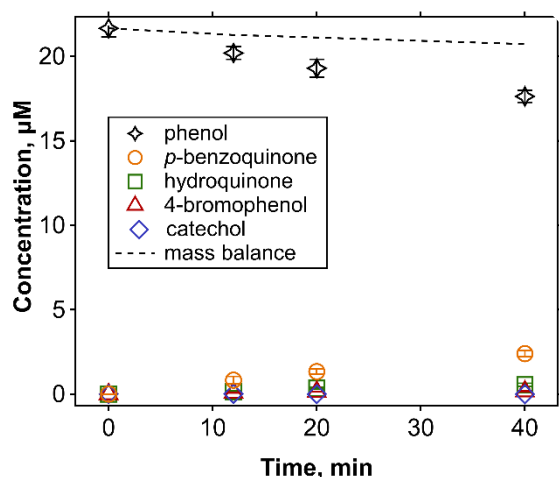


Figure S10. Concentrations of phenol and the identified products as a function of the γ -radiolysis time during the reaction of phenol with Br^\bullet , for the condition with 22 μM phenol, 0.7 mM 1,2-dibromoethane, 40 mM *t*-butanol, and 50 mM phosphate buffer (pH 7.1). See Figure 2 (main text) for relative product formation.

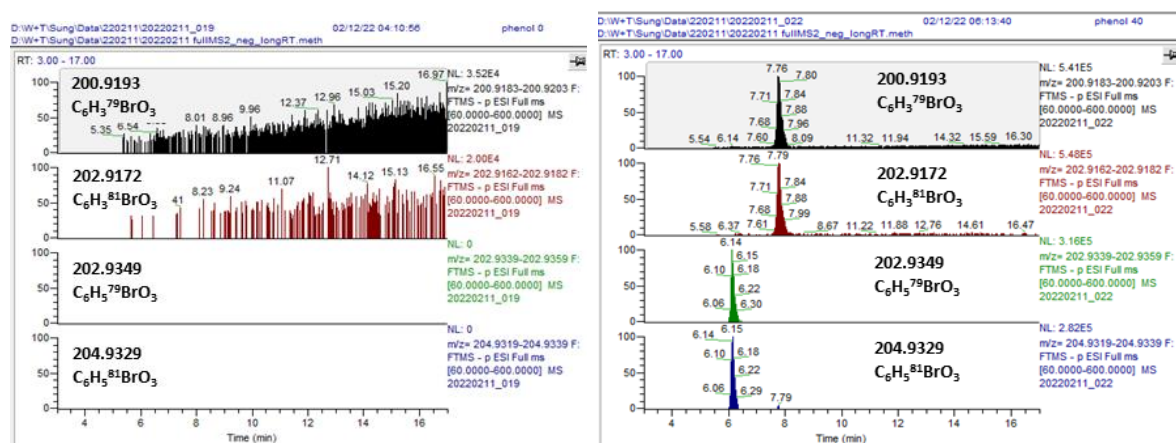


Figure S11. Left: Filtered chromatograms of a blank sample (no γ -radiolysis); right: γ -radiolysis sample ($t = 40$ min) with exact masses of 200.9193, 202.9172, 202.9349, and 204.9329 (from top to bottom of the chromatograms) corresponding to the molecular formulas of $\text{C}_6\text{H}_5^{79}\text{BrO}_3$, $\text{C}_6\text{H}_5^{81}\text{BrO}_3$, $\text{C}_6\text{H}_5^{79}\text{BrO}_3$, and $\text{C}_6\text{H}_5^{81}\text{BrO}_3$.

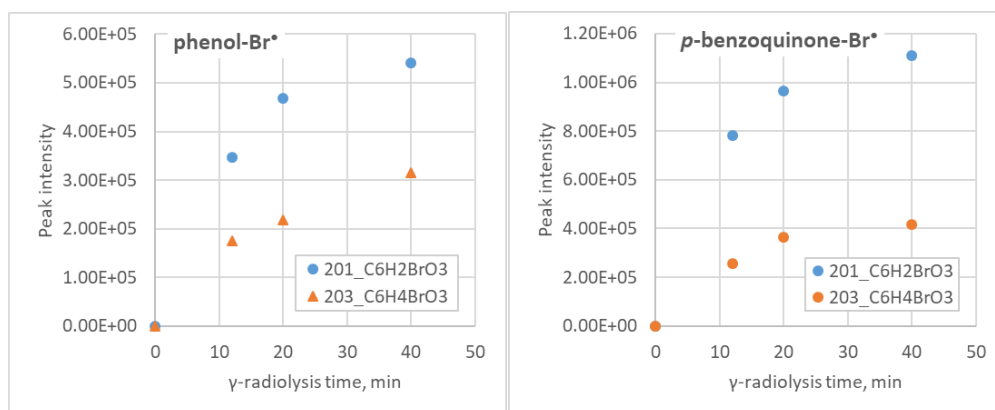


Figure S12. Trends of the peak intensity as a function of the γ -radiolysis time for the exact masses of 200.9193 (blue circles, corresponding to $C_6H_2^{79}BrO_3$ as M-H) and 202.9349 (orange triangles, corresponding to $C_6H_4^{79}BrO_3$ as M-H) during the reaction of Br^* with phenol (left) or *p*-benzoquinone (right).

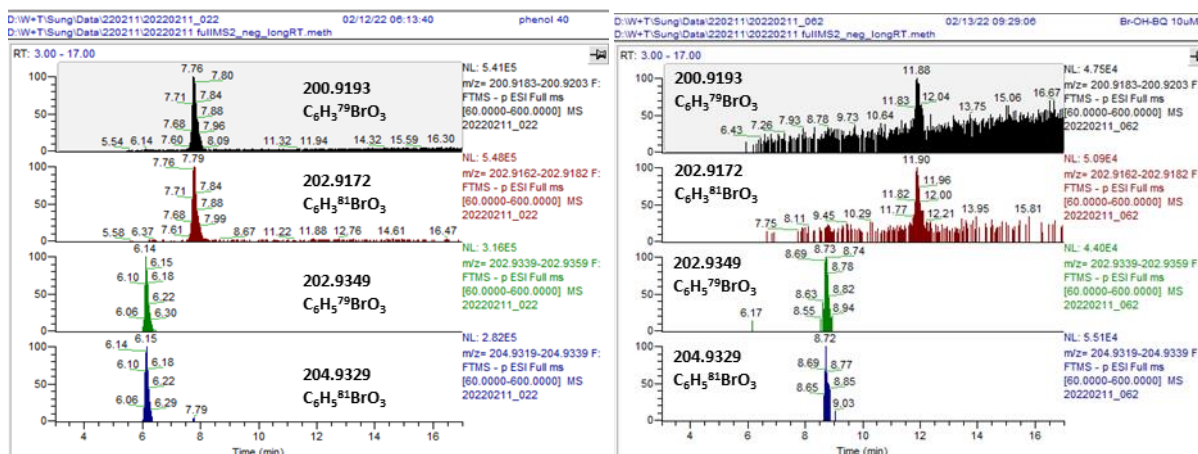


Figure S13. Left: Filtered chromatograms of a γ -radiolysis sample ($t = 40$ min); right: synthesized substituted *p*-benzoquinone with the exact masses of 200.9193, 202.9172, 202.9349, and 204.9329 (from top to bottom of the chromatograms) as [M-H], corresponding to the molecular formulas $C_6H_3^{79}BrO_3$, $C_6H_3^{81}BrO_3$, $C_6H_5^{79}BrO_3$, and $C_6H_5^{81}BrO_3$. Retention times for $C_6H_3BrO_3$, and $C_6H_5BrO_3$ are 7.8 and 6.1 min for the γ -radiolysis sample (left) and 11.9 and 8.7 min for the synthesized chemical (right).

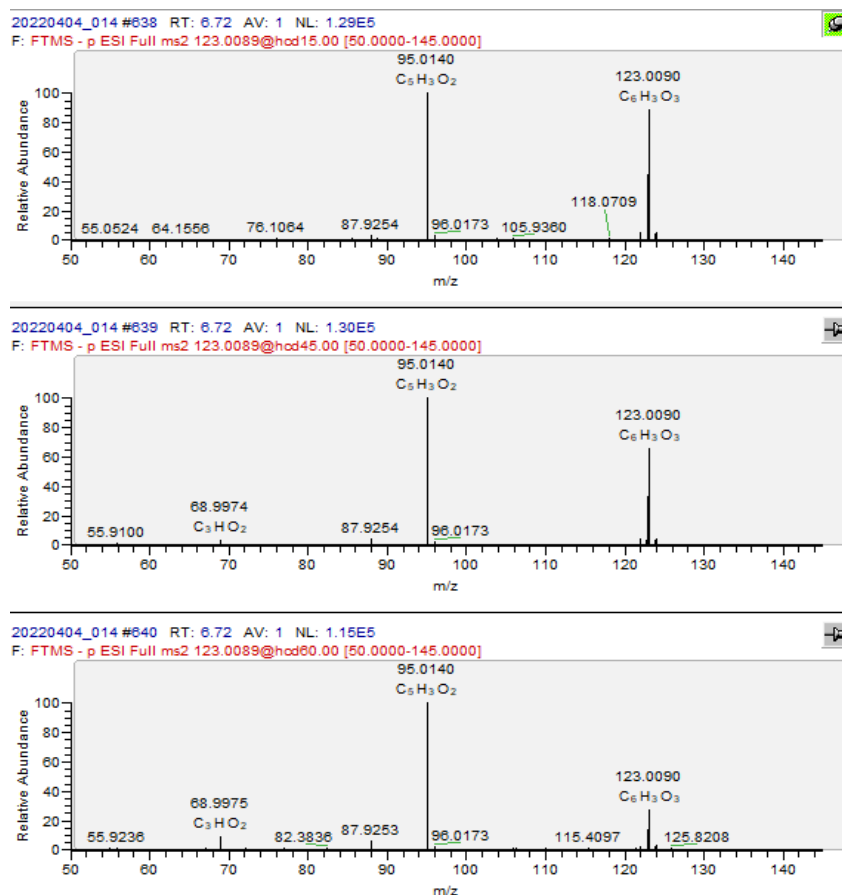


Figure S14. MS² spectra of m/z of 123.0089 (as [M-H]) with a HCD normalized collision energy (unitless) of 15 (top), 45 (middle), or 60 (bottom).

Suspected precursor structures	Suspected fragment structure 1		Suspected fragment structure 2	
Formula C ₆ H ₃ O ₃ Mass 123.0089 (as M-H)	Formula [C ₃ H ₂ O ₂]-H- Mass 68.9982 Peak m/z 68.9974	Formula [C ₅ H ₄ O ₂]-H- Mass 95.0139 Peak m/z 95.0140	Formula [C ₃ H ₂ O ₂]-H- Mass 68.9982 Peak m/z 68.9974	Formula [C ₅ H ₄ O ₂]-H- Mass 95.0139 Peak m/z 95.0140

Figure S15. Simulated fragment ions corresponding to the detected major daughter ions of m/z = 95.0140 and 68.9974. Two different suspected structures are shown for the parent ion of 123.0089 as [M-H]. The fragment ions were obtained based on an *in silico* fragmentation simulation by MetFrag.⁴⁸

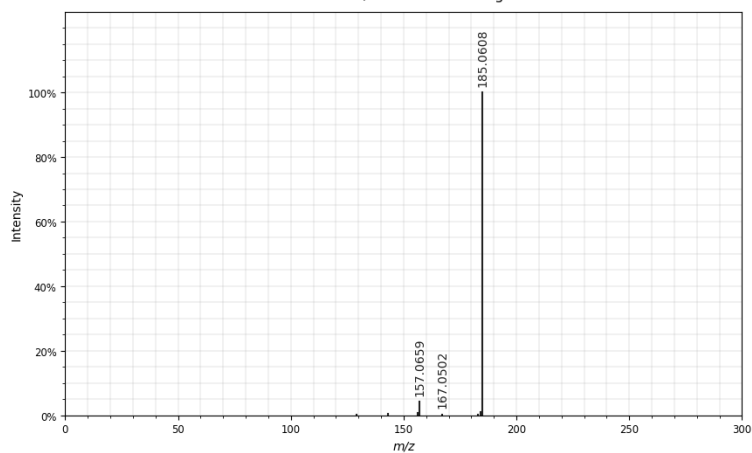
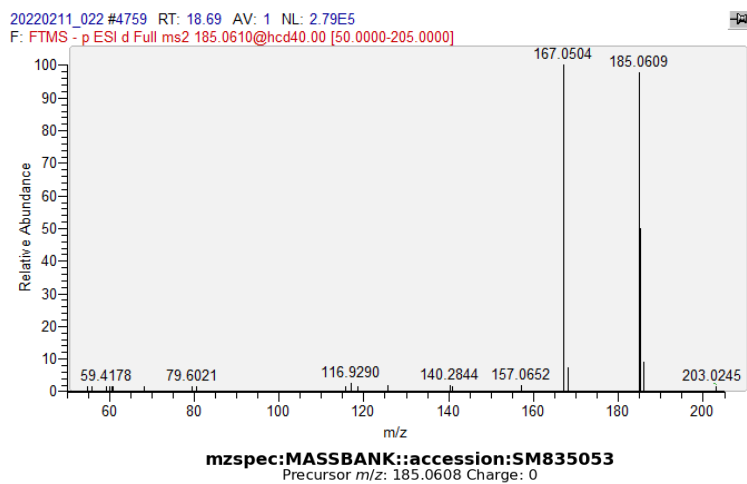


Figure S16. Top: Measured; bottom: reported MS² spectra for the exact masses of 185.0610 and 185.0608, respectively (both corresponding to C₁₂H₉O₂ as M-H). The reported MS² spectrum was obtained from <https://massbank.eu/MassBank/>.⁴⁹

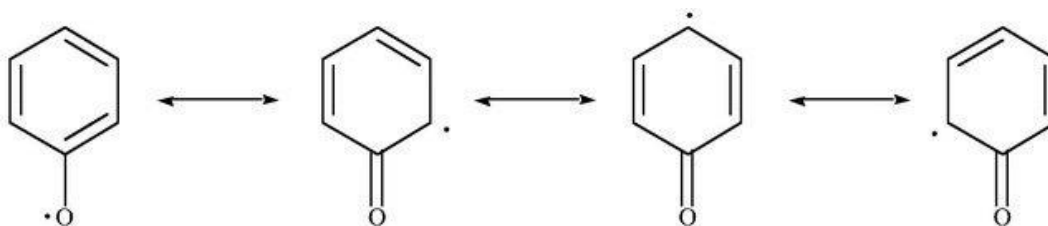


Figure S17. Resonance structures of the phenoxyl radical.

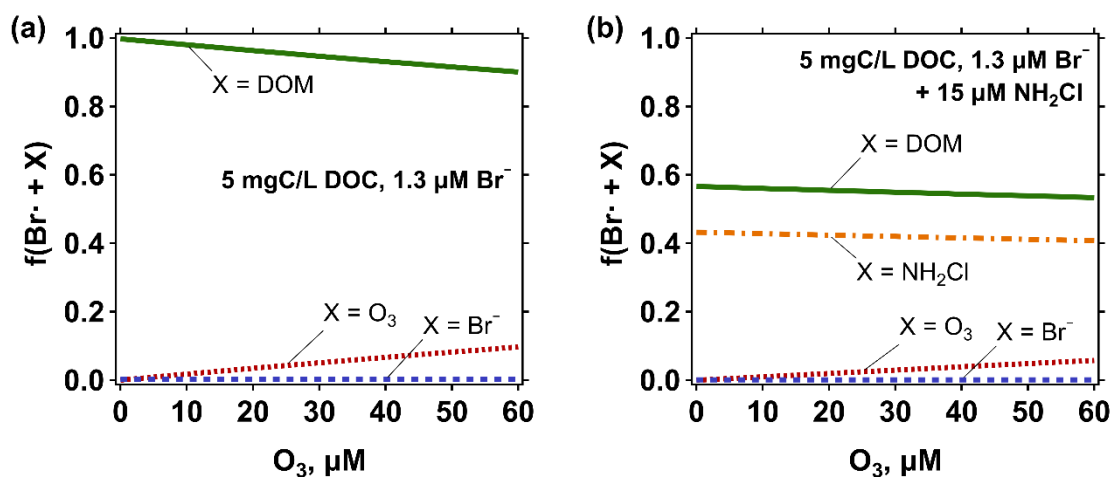


Figure S18. Calculated fractions of Br^* reacting with DOM (green line), ozone (red line), bromide (blue line), or NH_2Cl (orange line) as a function of the ozone concentration in (a) absence or (b) presence of NH_2Cl . The selected concentrations were 5 mgC/L DOC, 1.3 μM Br^- (100 $\mu\text{g/L}$ Br^-), and 15 μM NH_2Cl .

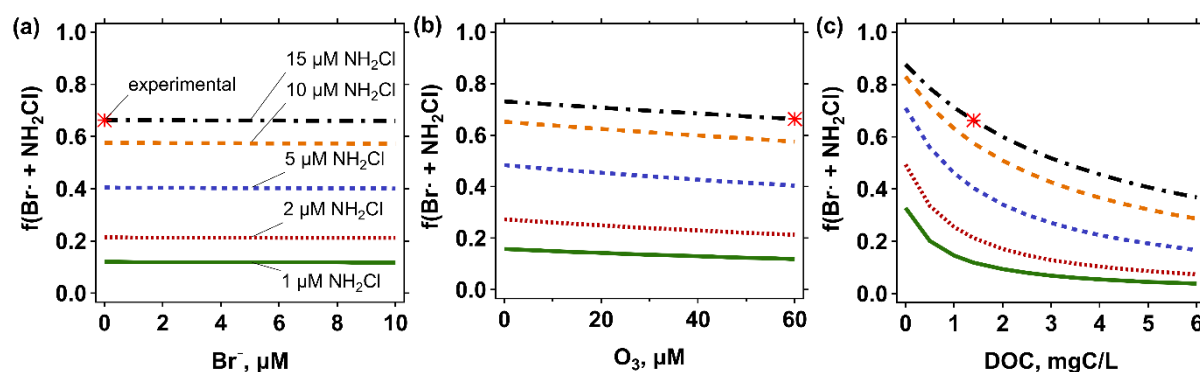


Figure S19. Calculated fractions of Br^* reacting with NH_2Cl as a function of (a) bromide, (b) ozone, or (c) DOC concentration. Lines indicate modelled NH_2Cl concentrations (1, 2, 5, 10, and 15 μM) and an asterisk symbol indicates the conditions applied in the ozonation experiment. Bromide, ozone, and DOC concentrations were fixed at 2 μM , 60 μM , and 1.4 mgC/L (corresponding to the experimental conditions) when they were not an independent variable of the plot.

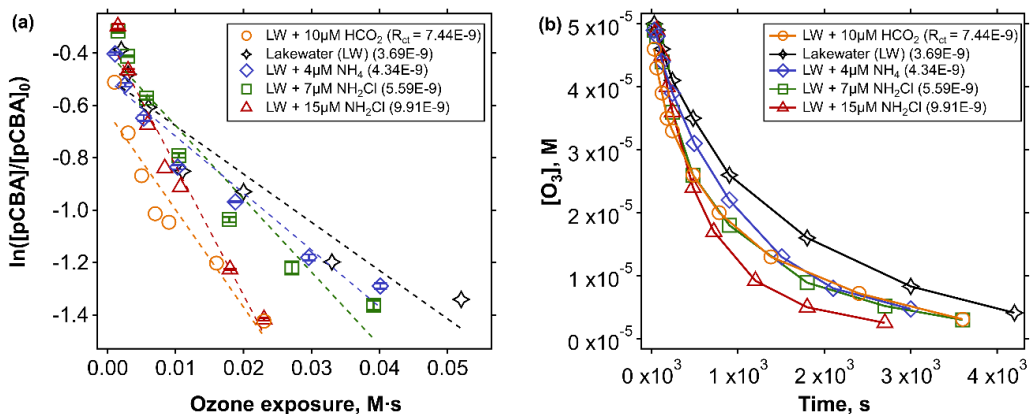


Figure S20. (a) *p*CBA abatement as a function of the ozone exposure and (b) ozone decrease as a function of reaction time, for ozonation of Lake Zurich water (1.4 mgC/L DOM, 2 μM bromide, 1 mM phosphate buffer (pH 7.6), 5 μM *p*CBA, and an ozone dose of 60 μM in absence or presence of an additional agent (10 μM formate, 4 μM ammonium, 7 μM NH₂Cl, or 15 μM NH₂Cl). The numbers in parentheses in the legend in plot (a) indicate the R_{ct} derived from the slopes of the regression lines.

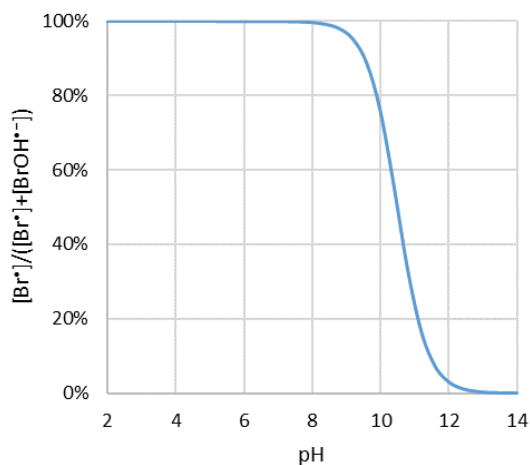
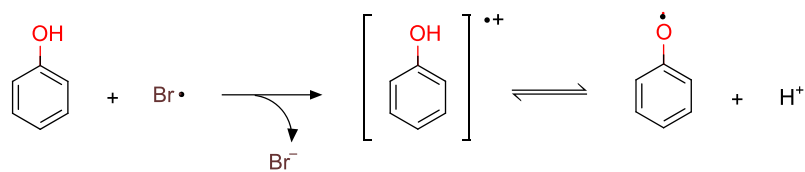
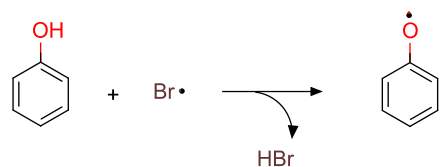


Figure S21. Fraction of Br^* in equilibrium with $BrOH^{*-}$ as a function of pH.

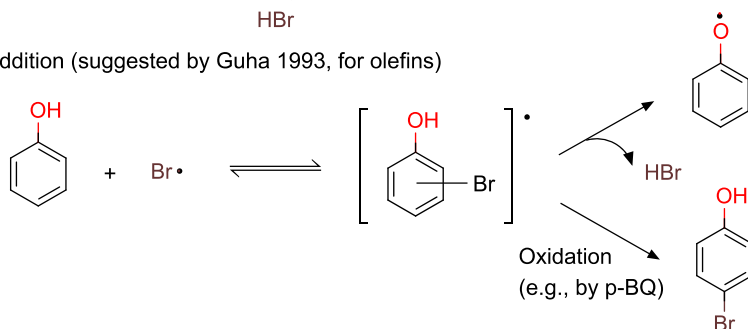
(1) Electron transfer (supported by QC data)



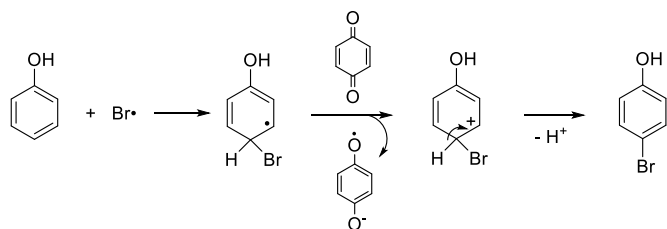
(2) H-abstraction (suggested by Merényi and Lind 1994, for alcohols)



(3) Addition (suggested by Guha 1993, for olefins)



Detailed mechanism of the oxidation step of (3):



Scheme S1. Possible initial reaction pathways for the reaction of phenol with Br^\bullet .

References

- (1) Hand, V. C.; Margerum, D. W. Kinetics and Mechanisms of the Decomposition of Dichloramine in Aqueous Solution. *Inorg. Chem.* **1983**, *22* (10), 1449–1456. <https://doi.org/10.1021/ic00152a007>.
- (2) Essaïed, K.-A.; Brown, L. V.; von Gunten, U. Reactions of Amines with Ozone and Chlorine: Two Novel Oxidative Methods to Evaluate the N-DBP Formation Potential from Dissolved Organic Nitrogen. *Water Research* **2022**, *209*, 117864. <https://doi.org/10.1016/j.watres.2021.117864>.
- (3) Walpen, N.; Houska, J.; Salhi, E.; Sander, M.; von Gunten, U. Quantification of the Electron Donating Capacity and UV Absorbance of Dissolved Organic Matter during Ozonation of Secondary Wastewater Effluent by an Assay and an Automated Analyzer. *Water Research* **2020**, *185*, 116235. <https://doi.org/10.1016/j.watres.2020.116235>.
- (4) Wenk, J.; Aeschbacher, M.; Salhi, E.; Canonica, S.; von Gunten, U.; Sander, M. Chemical Oxidation of Dissolved Organic Matter by Chlorine Dioxide, Chlorine, And Ozone: Effects on Its Optical and Antioxidant Properties. *Environ. Sci. Technol.* **2013**, *47* (19), 11147–11156. <https://doi.org/10.1021/es402516b>.
- (5) Rougé, V.; von Gunten, U.; Allard, S. Efficiency of Pre-Oxidation of Natural Organic Matter for the Mitigation of Disinfection Byproducts: Electron Donating Capacity and UV Absorbance as Surrogate Parameters. *Water Research* **2020**, 116418. <https://doi.org/10.1016/j.watres.2020.116418>.
- (6) Donati, A. Spectroscopic and Kinetic Investigations of Halogen Containing Radicals in the Tropospheric Aqueous Phase, University of Leipzig, Leipzig, Germany, 2002. <http://d-nb.info/967494907>.
- (7) Ershov, B. G.; Kelm, M.; Gordeev, A. V.; Janata, E. A Pulse Radiolysis Study of the Oxidation of Br⁻ by Cl₂⁻ in Aqueous Solution: Formation and Properties of ClBr⁻. *Phys. Chem. Chem. Phys.* **2002**, *4* (10), 1872–1875. <https://doi.org/10.1039/B110362H>.
- (8) Valentine, R. L.; Brandt, K. I.; Jafvert, C. T. A Spectrophotometric Study of the Formation of an Unidentified Monochloramine Decomposition Product. *Water Research* **1986**, *20* (8), 1067–1074. [https://doi.org/10.1016/0043-1354\(86\)90051-5](https://doi.org/10.1016/0043-1354(86)90051-5).
- (9) 4500-Cl Chlorine (Residual). In *Standard method for examination of water and wastewater*; American Public Health Association (APHA).
- (10) von Gunten, U.; Oliveras, Y. Advanced Oxidation of Bromide-Containing Waters: Bromate Formation Mechanisms. *Environ. Sci. Technol.* **1998**, *32* (1), 63–70. <https://doi.org/10.1021/es970477j>.
- (11) Allen, A. O.; Hochanadel, C. J.; Ghormley, J. A.; Davis, T. W. Decomposition of Water and Aqueous Solutions Under Mixed Fast Neutron and Gamma Radiation. *The Journal of Physical Chemistry* **1952**, *56* (5), 575–586.
- (12) Lal, M.; Mahal, H. S. Reactions of Alkylbromides with Free Radicals in Aqueous Solutions. *International Journal of Radiation Applications and Instrumentation. Part C. Radiation Physics and Chemistry* **1992**, *40* (1), 23–26. [https://doi.org/10.1016/1359-0197\(92\)90134-2](https://doi.org/10.1016/1359-0197(92)90134-2).
- (13) Merényi, G.; Lind, J. Reaction Mechanism of Hydrogen Abstraction by the Bromine Atom in Water. *J. Am. Chem. Soc.* **1994**, *116* (17), 7872–7876. <https://doi.org/10.1021/ja00096a050>.
- (14) Guha, S. N.; Schoneich, C.; Asmus, K. D. Free Radical Reductive Degradation of Vic-Dibromoalkanes and Reaction of Bromine Atoms with Polyunsaturated Fatty Acids: Possible Involvement of Br[•] in the 1,2-Dibromoethane-Induced Lipid-Peroxidation. *Archives of Biochemistry and Biophysics* **1993**, *305* (1), 132–140. <https://doi.org/10.1006/abbi.1993.1402>.
- (15) Lal, M.; Mönig, J.; Asmus, K.-D.; Wardman, P. Free Radical Induced Degradation of 1, 2-Dibromoethane. Generation of Free Br⁺ Atoms. *Free Radical Research Communications* **1986**, *1* (4), 235–241. <https://doi.org/10.3109/10715768609051633>.
- (16) Klänning, U. K.; Wolff, T. Laser Flash Photolysis of HClO, ClO⁻, HBrO, and BrO⁻ in Aqueous Solution. Reactions of Cl⁻ and Br⁻ Atoms. *Berichte der Bunsengesellschaft für physikalische Chemie* **1985**, *89* (3), 243–245. <https://doi.org/10.1002/bbpc.19850890309>.

- (17) Nauser, T.; Carreras, A. Carbon-Centered Radicals Add Reversibly to Histidine – Implications. *Chem. Commun.* **2014**, *50* (92), 14349–14351. <https://doi.org/10.1039/C4CC05316H>.
- (18) Beaumont, P. C.; Powers, E. L. Radiation Sensitivity of DNA-Metal Complexes: A Pulse Radiolysis Study. *International Journal of Radiation Biology and Related Studies in Physics, Chemistry and Medicine* **1983**, *43* (5), 485–494. <https://doi.org/10.1080/09553008314550581>.
- (19) Armstrong, D. A.; Huie, R. E.; Koppenol, W. H.; Lymar, S. V.; Merényi, G.; Neta, P.; Ruscic, B.; Stanbury, D. M.; Steenken, S.; Wardman, P. Standard Electrode Potentials Involving Radicals in Aqueous Solution: Inorganic Radicals (IUPAC Technical Report). *Pure and Applied Chemistry* **2015**, *87* (11–12), 1139–1150. <https://doi.org/10.1515/pac-2014-0502>.
- (20) Zhang, H.; Mostafavi, M. UV-Absorption Observation of the Silver Bromide Growth from a Single Molecule to the Crystal in Solution. *J. Phys. Chem. B* **1997**, *101* (42), 8443–8448. <https://doi.org/10.1021/jp9712821>.
- (21) von Sonntag, C.; von Gunten, U. *Chemistry of Ozone in Water and Wastewater Treatment*; IWA Publishing, 2012.
- (22) Marenich, A. V.; Cramer, C. J.; Truhlar, D. G. Universal Solvation Model Based on Solute Electron Density and on a Continuum Model of the Solvent Defined by the Bulk Dielectric Constant and Atomic Surface Tensions. *The Journal of Physical Chemistry B* **2009**, *113* (18), 6378–6396. <https://doi.org/10.1021/jp810292n>.
- (23) Zhao, Y.; Truhlar, D. G. The M06 Suite of Density Functionals for Main Group Thermochemistry, Thermochemical Kinetics, Noncovalent Interactions, Excited States, and Transition Elements: Two New Functionals and Systematic Testing of Four M06-Class Functionals and 12 Other Functionals. *Theoretical Chemistry Accounts* **2008**, *120* (1), 215–241. <https://doi.org/10.1007/s00214-007-0310-x>.
- (24) Bryantsev, V. S.; Diallo, M. S.; Goddard III, W. A. Calculation of Solvation Free Energies of Charged Solutes Using Mixed Cluster/Continuum Models. *J. Phys. Chem. B* **2008**, *112* (32), 9709–9719. <https://doi.org/10.1021/jp802665d>.
- (25) Tomaník, L.; Muchová, E.; Slavíček, P. Solvation Energies of Ions with Ensemble Cluster-Continuum Approach. *Phys. Chem. Chem. Phys.* **2020**, *22* (39), 22357–22368. <https://doi.org/10.1039/D0CP02768E>.
- (26) Purvis, G. D.; Bartlett, R. J. A Full Coupled-cluster Singles and Doubles Model: The Inclusion of Disconnected Triples. *J. Chem. Phys.* **1982**, *76* (4), 1910–1918. <https://doi.org/10.1063/1.443164>.
- (27) Montgomery, J. A.; Frisch, M. J.; Ochterski, J. W.; Petersson, G. A. A Complete Basis Set Model Chemistry. VI. Use of Density Functional Geometries and Frequencies. *The Journal of Chemical Physics* **1999**, *110* (6), 2822–2827. <https://doi.org/10.1063/1.477924>.
- (28) Montgomery, J. A.; Frisch, M. J.; Ochterski, J. W.; Petersson, G. A. A Complete Basis Set Model Chemistry. VII. Use of the Minimum Population Localization Method. *J. Chem. Phys.* **2000**, *112* (15), 6532–6542. <https://doi.org/10.1063/1.481224>.
- (29) Wavefunction, Inc. Wavefunction, I. Spartan'18, 2018.
- (30) Halgren, T. A.; Nachbar, R. B. Merck Molecular Force Field. IV. Conformational Energies and Geometries for MMFF94. *Journal of Computational Chemistry* **1996**, *17* (5–6), 587–615. [https://doi.org/10.1002/\(SICI\)1096-987X\(199604\)17:5/6<587::AID-JCC4>3.0.CO;2-Q](https://doi.org/10.1002/(SICI)1096-987X(199604)17:5/6<587::AID-JCC4>3.0.CO;2-Q).
- (31) Marcus, R. A. Chemical and Electrochemical Electron-Transfer Theory. *Annual Review of Physical Chemistry* **1964**, *15* (1), 155–196. <https://doi.org/10.1146/annurev.pc.15.100164.001103>.
- (32) Raghavan, N. V.; Steenken, S. Electrophilic Reaction of the Hydroxyl Radical with Phenol. Determination of the Distribution of Isomeric Dihydroxycyclohexadienyl Radicals. *J. Am. Chem. Soc.* **1980**, *102* (10), 3495–3499. <https://doi.org/10.1021/ja00530a031>.
- (33) Acero, J. L.; Piriou, P.; von Gunten, U. Kinetics and Mechanisms of Formation of Bromophenols during Drinking Water Chlorination: Assessment of Taste and Odor Development. *Water Research* **2005**, *39* (13), 2979–2993. <https://doi.org/10.1016/j.watres.2005.04.055>.

- (34) Tee, O. S.; Paventi, M.; Bennett, J. M. Kinetics and Mechanism of the Bromination of Phenols and Phenoxide Ions in Aqueous Solution. Diffusion-Controlled Rates. *J. Am. Chem. Soc.* **1989**, *111* (6), 2233–2240. <https://doi.org/10.1021/ja00188a044>.
- (35) Buffle, M.-O.; Galli, S.; von Gunten, U. Enhanced Bromate Control during Ozonation: The Chlorine-Ammonia Process. *Environ. Sci. Technol.* **2004**, *38* (19), 5187–5195. <https://doi.org/10.1021/es0352146>.
- (36) Neemann, J.; Hulse, R.; Rexing, D.; Wert, E. Controlling Bromate Formation: During Ozonation With Chlorine and Ammonia. *Journal - AWWA* **2004**, *96* (2), 26–28. <https://doi.org/10.1002/j.1551-8833.2004.tb10542.x>.
- (37) Haag, W. R.; Hoigné, J.; Bader, H. Improved Ammonia Oxidation by Ozone in the Presence of Bromide Ion during Water Treatment. *Water Research* **1984**, *18* (9), 1125–1128. [https://doi.org/10.1016/0043-1354\(84\)90227-6](https://doi.org/10.1016/0043-1354(84)90227-6).
- (38) Poskrebyshev, G. A.; Huie, R. E.; Neta, P. Radiolytic Reactions of Monochloramine in Aqueous Solutions. *J. Phys. Chem. A* **2003**, *107* (38), 7423–7428. <https://doi.org/10.1021/jp030198k>.
- (39) Gleason, J. M.; McKay, G.; Ishida, K. P.; Mezyk, S. P. Temperature Dependence of Hydroxyl Radical Reactions with Chloramine Species in Aqueous Solution. *Chemosphere* **2017**, *187*, 123–129. <https://doi.org/10.1016/j.chemosphere.2017.08.053>.
- (40) Lei, Y.; Lei, X.; Westerhoff, P.; Tong, X.; Ren, J.; Zhou, Y.; Cheng, S.; Ouyang, G.; Yang, X. Bromine Radical ($\text{Br}\cdot$ and $\text{Br}_2\cdot^-$) Reactivity with Dissolved Organic Matter and Brominated Organic Byproduct Formation. *Environ. Sci. Technol.* **2022**, *56* (8), 5189–5199. <https://doi.org/10.1021/acs.est.2c00549>.
- (41) Zhan, C.-G.; Dixon, D. A. Hydration of the Fluoride Anion: Structures and Absolute Hydration Free Energy from First-Principles Electronic Structure Calculations. *J. Phys. Chem. A* **2004**, *108* (11), 2020–2029. <https://doi.org/10.1021/jp0311512>.
- (42) Tissandier, M. D.; Cowen, K. A.; Feng, W. Y.; Gundlach, E.; Cohen, M. H.; Earhart, A. D.; Coe, J. V.; Tuttle, T. R. The Proton's Absolute Aqueous Enthalpy and Gibbs Free Energy of Solvation from Cluster-Ion Solvation Data. *J. Phys. Chem. A* **1998**, *102* (40), 7787–7794. <https://doi.org/10.1021/jp982638r>.
- (43) Wardman, P. Reduction Potentials of One-Electron Couples Involving Free Radicals in Aqueous Solution. *Journal of Physical and Chemical Reference Data* **1989**, *18* (4), 1637–1755. <https://doi.org/10.1063/1.555843>.
- (44) Pearson, R. G. Ionization Potentials and Electron Affinities in Aqueous Solution. *J. Am. Chem. Soc.* **1986**, *108* (20), 6109–6114. <https://doi.org/10.1021/ja00280a002>.
- (45) Jonsson, M.; Lind, J.; Reitberger, T.; Eriksen, T. E.; Merenyi, G. Redox Chemistry of Substituted Benzenes: The One-Electron Reduction Potentials of Methoxy-Substituted Benzene Radical Cations. *J. Phys. Chem.* **1993**, *97* (43), 11278–11282. <https://doi.org/10.1021/j100145a027>.
- (46) Lal, M. Free $\dot{\text{B}}\text{r}$ Atom and Free Radical Reactions in the Radiolysis of 1,2-Dibromoethane (DBE) and Other Bromohydrocarbons in Air-Free Aqueous Solutions. *International Journal of Radiation Applications and Instrumentation. Part C. Radiation Physics and Chemistry* **1988**, *32* (6), 741–745. [https://doi.org/10.1016/1359-0197\(88\)90161-0](https://doi.org/10.1016/1359-0197(88)90161-0).
- (47) Buxton, G. V.; Greenstock, C. L.; Helman, W. P.; Ross, A. B. Critical Review of Rate Constants for Reactions of Hydrated Electrons, Hydrogen Atoms and Hydroxyl Radicals ($\cdot\text{OH}/\cdot\text{O}^-$ in Aqueous Solution. *Journal of Physical and Chemical Reference Data* **1988**, *17* (2), 513–886. <https://doi.org/10.1063/1.555805>.
- (48) Ruttkies, C.; Schymanski, E. L.; Wolf, S.; Hollender, J.; Neumann, S. MetFrag Relaunch: Incorporating Strategies beyond in Silico Fragmentation. *J. Cheminform* **2016**, *8* (1), 3. <https://doi.org/10.1186/s13321-016-0115-9>.
- (49) Schulze, T.; Meier, R.; Alygizakis, N.; Schymanski, E.; Bach, E.; D.H. Li; Lauperbe; Raalizadeh; Tanaka, S.; Witting, M. MassBank/MassBank-Data: Release Version 2021.12, 2021. <https://doi.org/10.5281/ZENODO.5775684>.